Correlated ion stopping in plasmas

Günter Zwicknagel and Claude Deutsch
Laboratoire de Physique des Gaz et des Plasmas, Bâtiment 212, Université Paris XI, 91405 Orsay, France
(Received 13 January 1997; revised manuscript received 6 March 1997)

The basic features of correlated ion stopping in plasmas are demonstrated by employing two opposite extremes of cluster structures, a statistical model with a spatial ion distribution of Gaussian shape and the highly regular configuration of N-ion chains and cubic boxes. In the case of the ion chains the resonant character of correlated stopping due to the interference of the excited wake fields is discussed in detail. The general behavior of correlation effects is summarized and its dependence on the ratio of cluster size and interion spacing to the screening length in the plasma, as well as the ratio of the cluster velocity to the mean electron velocity in the target, is stressed out. The validity and applicability of the dielectric response formalism used for describing correlated stopping is critically reviewed. A scheme is presented to extend the linear formalism to weak nonlinear situations that occur, in particular, for small highly charged clusters at moderate or low velocities. For the Gaussian cluster a fit formula is given, which allows a fast and accurate calculation of the enhancement of stopping due to correlation effects and applies for all degrees of degeneracy of the electrons and arbitrary cluster velocities. [S1063-651X(97)00907-0]

PACS number(s): 52.40.Mj, 34.50.Bw

I. INTRODUCTION

The interaction of fullerenelike, carbonlike, or metallic clusters with solids and hot plasma targets has recently attracted a lot of attention concerning the investigation of the cluster structures themselves, as well as the use of cluster-ion beams (CIB) as drivers to compress the target and to produce high energy densities in matter. In this context CIB are proposed as a promising driver for heavy ion inertial fusion (ICF) [1,2]. There the interest is mainly in particles with energies of a few keV per nucleon which interact mostly with the target electrons. Because such clusters will fragment quickly on a femtosecond time scale when hitting the target, one has to consider an ion debris with some atomic units relative distances between the ions. Within the dielectric formalism the correlation effects on the stopping, in such situations, were already submitted to a number of investigations, first on dicluster stopping [3], later on arbitrarily large N clusters [1,4–6]. While in these works the target was a fully degenerate electron jellium, recent investigations also addressed the cases of partially degenerate plasmas [7] and classical electron plasmas [8–10] as well. Also, at variance with the dielectric linear response description, nonperturbative approaches have been used to study dicluster stopping at low velocities and in fully degenerate electron targets [11,12].

To investigate the effects of correlated stopping in a CIB driven ICF scenario a wide range of target conditions for the ion or ion-cluster interaction within the absorber or converter have to be considered. Due to the enormous heating, one starts with a solid (jellium) target in the beginning of the ion-beam pulse which turns a partially degenerate plasma into a dense, high temperature, and classical plasma. To cover the full width of target conditions and phenomena involved in correlated ion stopping we concentrate in this paper on a general qualitative discussion of correlated ion stopping and a review on the involved basic features rather than devoting us to very specific situations as already addressed in the literature. The basic phenomena in correlated ion stopping are demonstrated in Sec. III by employing three generic examples of cluster structures, Gaussian clusters, N chains of ions, and ions on the vertices of cubic boxes. In the Gaussian cluster the ions are distributed around the cluster center at distances according to a Gaussian-like probability as a statistical description for the ion debris created by the fragmentation process. In contrast to such a statistical model for the cluster structure the N-ion chains and the cubic boxes ion arrangements represent the opposite extreme of a well-defined highly regular ion configuration which may exhibit additional phenomena due to possible interferences in the excited wake fields. As will be outlined, the quality and quantity of the basic correlation effects are mainly determined by the ratio of the typical length scale of or in the ion cluster (λ_c) compared with the screening length of the target plasma (λ_s) and the ratio of the ion-cluster velocity v to the mean velocity $\langle v_e \rangle$ of the target electrons. The arrangement of several ions determines the polarization of the plasma and the creation of the induced electrical field and, thus, the correlation effects on the stopping power as the force on the ions due to the induced field at their locations. For typical ion interdistances and a size of the cluster small compared to the screening length in the target plasma (λ_s), the ions altogether create the target response. Thereby, the induced field is the same as one produced by a single large charge and yields an enhancement of the stopping. In the opposite case of large distances between the ions, with respect to the screening length, each ion acts, more or less, like an isolated ion on the target, however, the excited wake fields may interfere constructively or destructively and thereby enhance or reduce the stopping compared to the case of uncorrelated stopping. The different underlying physics yields different features of correlated stopping depending on the target conditions, the cluster velocities, and the number of ions in the cluster, as will be illustrated for the examples in Sec. III and summarized in a more general overview in Sec. IV. In Sec. II we briefly review the dielectric linear response formalism,

which we employ to describe correlated stopping, and critically discuss the validity and applicability of this commonly used approach. Further, we introduce a scheme to extend the linear response treatment of the stopping of ion clusters to a semilinear regime to account for (weak) nonlinear effects which become important, in particular, for small and highly charged clusters at moderate or low velocities. In addition, a fit formula for the enhancement of stopping for the Gaussian cluster is presented in Sec. III which is applicable for all degrees of degeneracy of the target plasma and any cluster velocity. This formula provides, besides a fast evaluation of the enhancement, a good understanding of the physics of correlated stopping. As a basis of future work, it allows a cheap but reliable estimate of the correlation effects on the range and energy deposition of ion debris, *including* the Coulomb explosion of the cluster, so far neglected here as in most of the published investigations on correlated stopping.

II. ION-CLUSTER STOPPING IN PLASMAS

The whole slowing down process of an ion cluster, after fragmentation and initial ionization have taken place, which are subjects of great interest by themselves, involves the stopping power on the cluster, the evolution of the charge states of the ions, and the Coulomb explosion. A description of ion-cluster stopping, hence, requires a simultaneous treatment of all these processes including besides correlation effects on the stopping power the, up to now open, questions of correlation effects on the charge states as well. Some first work on this task, ignoring correlation effects on the ion charges, is reported in [13,14] for the energy loss of C_{60} clusters. Here, we concentrate completely on the stopping power for a given cluster configuration, i.e., for given positions, velocities, and charge states of the ions, as it may occur at a certain time within the slowing down.

To investigate the basic aspects of correlated stopping we employ the dielectric linear response formalism [15,16]. There the stopping is determined from the electrical field induced in the target plasma by the charge distribution of the cluster $\rho(\mathbf{r},t)$ and the corresponding dynamical response for a momentum transfer $\mathbf{k}$ and an energy transfer ω is provided in terms of the dielectric function $\varepsilon(\mathbf{k},\omega)$. We only consider electronic stopping by an ideal free electron target with density n and temperature T, where the kinetic energy of the electrons always exceeds their potential energy and the ideality parameter ξ is smaller than unity, that is,

$$\xi=\frac{\langle E_p\rangle}{\langle E_k\rangle}=\frac{e^2}{4\pi\epsilon_0 a(E_F+k_BT)}=\frac{2\alpha^2 r_s}{1+\Theta}<1, \tag{1}$$

where $r_s=a/a_0$ with $a=(4\pi n/3)^{-1/3}$ and a_0 the Bohr radius, $\Theta=(k_BT)/E_F$ denotes the degree of degeneracy, E_F the Fermi energy, and $\alpha=(4/9\pi)^{1/3}=0.521\ldots$. For classical plasmas $\Theta\gg1$, the parameter ξ turns into the classical plasma parameter $\Gamma=e^2/4\pi\epsilon_0 k_BTa=2\alpha^2 r_s/\Theta$. Rewriting the condition $\xi<1$ as an inequality for the temperature, we have

$$\frac{k_BT}{13.6\ \text{eV}}>\frac{2\alpha^2 r_s-1}{\alpha^2 r_s^2}, \tag{2}$$

and an ideal target for electron densities $n>2.6\times10^{23}\ \text{cm}^{-3}$ ($r_s<1/2\alpha^2\approx1.84$) *or* temperatures $T>3.7$ eV. Hence, except for the very early time of heating an ICF target by an (cluster-) ion beam, we deal with an ideal electron target. Within the boundaries given by the condition $\xi<1$, we, however, allow in our considerations for any degree of degeneracy Θ, to include classical plasmas as well as the electron jellium in solids. For these ideal plasmas we can use the dielectric function $\varepsilon(\mathbf{k},\omega)$ determined in the well-known random phase approximation (RPA) for free electron targets at any degeneracy (e.g., [17]).

A. Dielectric linear response formalism

Within the dielectric formalism, the external charge density

$$\rho(\mathbf{r},t)=\int d^3r'\rho(\mathbf{r}')\,\delta^3(\mathbf{r}'-(\mathbf{r}-\mathbf{v}t))$$

$$=\sum_i Z_ie\,\delta^3(\mathbf{r}_i-(\mathbf{r}-\mathbf{v}t)) \tag{3}$$

of an ion-cluster projectile of N pointlike ions with charges $\{Z_ie\}$ located at $\{\mathbf{r}_i\}$, which all move through the target with the same projectile velocity $\mathbf{v}$ (''frozen configuration'' of relative positions), results in the general expression for the stopping power $S=-dE/ds$ [7,18], where dE/ds is the change of the projectile energy per unit path length,

$$S=\frac{1}{\epsilon_0(2\pi)^3}\int d^3k\frac{\mathbf{k}\cdot\hat{\mathbf{v}}}{k^2}\,\mathrm{Im}\left[\frac{-1}{\varepsilon(\mathbf{k},\mathbf{k}\cdot\mathbf{v})}\right]\tilde{\rho}(-\mathbf{k})\tilde{\rho}(\mathbf{k}). \tag{4}$$

Here, $\tilde{\rho}(\mathbf{k})$ is the Fourier-transformed charge density $\rho(\mathbf{r})$ and

$$\tilde{\rho}_q(-\mathbf{k})\tilde{\rho}_q(\mathbf{k})=e^2\Bigg[\sum_n Z_n^2+\sum_n\sum_{m\neq n}Z_nZ_m$$

$$\times\exp[i\mathbf{k}\cdot(\mathbf{r}_n-\mathbf{r}_m)]\Bigg]. \tag{5}$$

The use of pointlike ions in Eqs. (3)–(5) serves to restrict the forthcoming discussion to the basic phenomena and represents real ions of extension d, if d is small compared to the wavelengths of the electrons, $\lambda\!\!\!^{-}_r=\hbar/m\langle v_r\rangle\gg d$, where $\langle v_r\rangle$ is the relative velocity $\langle v_r\rangle=\langle|\mathbf{v}_e-\mathbf{v}|\rangle$, averaged over the electron distribution $f(\mathbf{v}_e)$. When the extension of the ions becomes important, non-point-like charge distributions of each ion $q_i(\mathbf{r})$, with $\int d^3r\ q_i(\mathbf{r})=Z_ie$ and $\rho(\mathbf{r})=\Sigma_i q_i(\mathbf{r}_i-\mathbf{r})$, can be introduced in the above description by replacing Eq. (3) through $\rho(\mathbf{r},t)=\Sigma_i q_i(\mathbf{r}_i-(\mathbf{r}-\mathbf{v}t))$ and $\tilde{\rho}(-\mathbf{k})\tilde{\rho}(\mathbf{k})=\Sigma_n\Sigma_m\exp[i\mathbf{k}\cdot(\mathbf{r}_n-\mathbf{r}_m)]q_n(-\mathbf{k})q_m(\mathbf{k})$ (see [7]).

For purposes of practical interest, as the determination of correlation effects on the heating of a target which is irradiated by a CIB, one wants to know the averaged stopping of an ion cluster rather than the stopping of individual clusters, which may differ in the detailed structure, the size, the orientation, the charge states of the ions, and so on. Hence, it is useful to study the average of Eq. (4) over an ensemble of

ion clusters with varying configurations $\{\mathbf{Z}_i\}$, $\{\mathbf{r}_i\}$. To simplify this further, we assume equal charges of the ions $Z_i=Z$, leading to the ensemble-averaged stopping per particle [4,5]

$$\langle S\rangle/N=\frac{Z^2e^2}{\epsilon_0(2\pi)^3}\int d^3k\frac{\mathbf{k}\cdot\hat{\mathbf{v}}}{k^2}\,\mathrm{Im}\left[\frac{-1}{\varepsilon(\mathbf{k},\mathbf{k}\cdot\mathbf{v})}\right]\Sigma(\mathbf{k}), \quad (6)$$

where $\Sigma(\mathbf{k})=\langle\tilde{\rho}(-\mathbf{k})\tilde{\rho}(\mathbf{k})\rangle/NZ^2e^2$ is the static structure factor of the ensemble of ion clusters. Introducing the pair-distribution function $g(\mathbf{r}_i-\mathbf{r}_j)$ of the ion clusters one gets

$$\Sigma(\mathbf{k})=1+\int d^3r\; g(\mathbf{r})\exp(-i\mathbf{k}\cdot\mathbf{r}), \quad (7)$$

with the normalization condition $\Sigma(\mathbf{k}=0)=1+\int d^3r\; g(\mathbf{r})=N$. It should be emphasized that the averaging procedure above yields an average on the stopping powers of an ensemble of clusters, and is not the stopping of an extended charge density $\langle\rho(\mathbf{r})\rangle$ resulting from an average on the cluster densities (3). The stopping of an extended charge distribution $\langle\rho(\mathbf{r})\rangle$ tends to zero in the limit of large clusters, that is, for a growing extension of the charge distribution $[\langle\rho(\mathbf{r})\rangle\to 0]$, while Eq. (6), in this case, approaches the stopping of isolated, individual ions $[g(\mathbf{r})\to 0,\Sigma(\mathbf{k})\to 1]$.

B. Applicability of the linear response treatment

Before proceeding further, we look briefly on the prerequisites to apply the widely used general approach (4) for the description of correlated stopping.

First of all, the employment of the linear response is only justified as long as the ion cluster represents a weak perturbation on the target plasma. For ion clusters of probably high total charges and rather moderate energies around 100 keV/u, nonlinear effects are a more serious problem than for very fast single ions. We shall discuss the validity of a linear response for ion clusters and in particular, the treatment of correlated stopping in a semilinear regime in Sec. II C.

The stopping power expression (4) implies that the induced electrical field in the comoving cluster frame is stationary on a time scale ω_p^{-1}, the inverse of the plasma frequency, and the response time of the electron target. To consider the stopping power (4) as a snapshot in the whole slowing down process allows only for changes in the cluster configuration and velocity, which are slow on this time scale. Besides slow changes $\dot{v}\propto S$ in the velocity v due to the stopping power S and changes $\dot{Z}$ in the charge states due to ionization and recombination, this further requires a sufficiently small spread $\mathbf{v}_i-\mathbf{v}$ in the velocities of the ions around the cluster mean velocity to avoid fast changes in the relative positions. While the first two processes undergo only slow variations in time for most cases of interest, it is not obvious that the velocity spread remains always small enough. The main sources for the velocity spread are the Coulomb explosion due to the repulsion of the ions, the straggling in the stopping power, various stopping powers caused by different ion charges of the cluster members, and also collisions with target ions.

The contribution to the velocity spread by the Coulomb explosion can be roughly estimated from the initial Coulomb energy of the ion cluster (when fragmentation and ionization have already taken place). For an ion cluster with N ions of (averaged) charge Ze and mass M, and an initial size r_0, the kinetic energy E_c (per u) gained by the ions during the repulsion is around

$$E_c\lesssim 0.0272\frac{Z^2N}{M/u}\left\langle\frac{a_0}{r_0}\right\rangle\ \mathrm{keV}, \quad (8)$$

where u is the atomic mass unit and a_0 is the Bohr radius. For most heavy ion clusters of interest, the energy E_c is much lower than the initial energy of the ions E_o (typically 10–1000 keV per u) and the corresponding spread of velocities is small compared to the actual cluster mean velocity v during the largest part of the slowing down.

The straggling strongly depends on the projectile velocity and target parameters as well as on correlations effects, mostly in a very similar manner as the stopping power [19] and no general statements on the importance of straggling on the velocity spread are available at present. In particular, it is not evident, that straggling is negligible in this context.

From different charge states of the ions, distributed around some mean value $\langle Z\rangle$, large changes in the individual velocities may be expected due to the strong dependence on the charge ($\dot{v}_i\propto Z_i^2$), in particular, for weakly charged projectiles where already small variations in the charge states yield large changes in stopping relative to the stopping in average.

While the contribution of nuclear stopping by the target ions is always negligible compared to the electronic stopping for the considered projectile velocities which are much higher than the thermal velocities of the target ions, their collisions with the projectile ions can, however, contribute significantly to the velocity spread of the cluster ions. To estimate the importance of this effect one has to compare the time scale of the cluster slowing with the time scale for such scattering events between the target ions (with density n_t and charge Z_te) and the projectile ions (with Ze) at the cluster velocity v. Disregarding the screening by the electrons, the corresponding collision rate ν can be obtained by using the Rutherford cross section, accounting for all collisions with, for example, deflection angles in the center of mass system larger than 90°. This rate $\nu=\pi n_t(Z_tZe^2/4\pi\epsilon_0\mu)^2v^{-3}$ (with the reduced mass μ) depends strongly on the charge states of the involved ions, as well as on the cluster velocity.

The evaluation of the amount of velocity spread needs detailed investigations. A first step extending the dielectric response description to clusters with small velocity spreads, which results in an explicitly time-dependent stopping power, was performed by Lontano and Raimondi [20] for hot and classical target plasmas. Despite open questions, postponed to a future work, we believe it reasonable for an overview on the features of correlated stopping to give all ions the same velocity $\mathbf{v}_i=\mathbf{v}$.

C. Validity of linear response for ion clusters

The linear response description (4) and (6), at present the most powerful theory to account for correlation effects in ion stopping, is restricted to weak perturbations of the target caused by the ion projectiles. In particular, for small ion

clusters with high total charge, this restriction may become a very serious one and has to be studied carefully. We first recall the condition for the validity of Eqs. (4) and (6) in the isolated single ion limit $[N=1,\Sigma(\mathbf{k})=1]$ and then extend these considerations to arbitrary ion distributions.

1. Weak coupling for single ions

To quantify the strength or degree of the perturbation on the target electrons as caused by a single ion, we first establish an estimate for the local potential energy $V_{ei}(r)$ of a target electron in the field of the moving ion by

$$V_{ei}(r)=\frac{Ze^2}{4\pi\epsilon_0 r}\left[1-\exp\left(-\frac{r}{\lambda\!\!\!^{-}_r}\right)\right]\exp\left(-\frac{r}{\lambda_s}\right). \tag{9}$$

Here the factor $\propto[1-\exp(-r/\lambda\!\!\!^{-}_r)]/r$ is a simple approximation for the expectation value of the electron-ion interaction $Ze^2/4\pi\epsilon_0 r$, when the electron is represented by a wave packet centered at distance r from the ion and of width $\lambda\!\!\!^{-}_r=\hbar/mv_r$ corresponding to the relative velocity $v_r=|\mathbf{v}_e-\mathbf{v}|$ (the reduced mass is replaced by the electron mass m for heavy projectiles). This factor accounts for quantum diffraction effects at short distances $\sim\lambda\!\!\!^{-}_r$, while the exponential factor $\exp(-r/\lambda_s)$ added on top accounts for the screening at large distances. Here we assume a velocity dependent screening length λ_s of the form $\lambda_s=\langle v_r\rangle/\omega_p$ for all densities and temperatures, where $\langle\ \rangle$ denotes the average over the electron distribution $f(\mathbf{v}_e)$ and $\omega_p=(e^2n/m\epsilon_0)^{1/2}$ the plasma frequency. The potential energy $V_{ei}(r)$ decays monotonically with increasing r for arbitrary $\lambda\!\!\!^{-}_r$ and λ_s. To avoid misinterpretation we emphasize that the approximative expression for the potential energy (9) will be used in the following to derive a definition of a linear, semilinear, and a nonlinear ion-target coupling regime, and to develop a correction to the linear response stopping for ion clusters in order to extend it from linear into semilinear regime. Expression (9) serves only this purpose, but does *not* enter the calculations of the stopping power as an effective ion-electron interaction. Thus its explicit form is of minor significance as long as both important physical phenomena, the wave nature of the electrons and the collective screening, are modeled sufficiently well. While screening results in a decay faster than $1/r$ on distances of the order of $\sim\lambda_s$, the wave nature of the electrons modifies the Coulomb potential on a scale $\sim\lambda\!\!\!^{-}_r$ resulting for decreasing r in a transition from the $1/r$ behavior to $V(r\to 0)\ \propto 1/\lambda\!\!\!^{-}_r$, when the wave packet is centered on the ion. This behavior is approximated by the simple exponential form $V(r)\propto[1-\exp(-r/\lambda\!\!\!^{-}_r)]/r$ (9). At low ion velocities this agrees with the well-known approximation for an effective ion-electron potential in the semiclassical limit [21], when the thermal velocity of the electrons is inserted as relative velocity v_r.

The projectile represents a weak perturbation on a target electron, if the potential energy from Eq. (9) is smaller than the energy of the electron, that is, the kinetic energy $mv_r^2/2$ (for ideal plasmas). From $V_{ei}(r)\leqslant mv_r^2/2$ we obtain the corresponding inequality

$$\varphi(r)=\frac{V_{ei}(r)}{mv_r^2}=\frac{b_0}{r}\left[1-\exp\left(-\frac{r}{\lambda\!\!\!^{-}_r}\right)\right]\exp\left(-\frac{r}{\lambda_s}\right)\leqslant\frac{1}{2}, \tag{10}$$

where b_0 is the classical collision diameter $b_0=Ze^2/(4\pi\epsilon_0 mv_r^2)$. Inspecting Eq. (10) we have to distinguish two situations.

(*a*) *The linear regime*. Since $V_{ei}(0)\geqslant V_{ei}(r)$, the local condition for a weak perturbation (10) is satisfied globally for

$$\eta=\frac{Ze^2}{4\pi\epsilon_0\hbar v_r}=\frac{b_0}{\lambda\!\!\!^{-}_r}=\lim_{r\to 0}\varphi(r)\leqslant\frac{1}{2}, \tag{11}$$

where we have introduced the Coulomb or Bloch parameter η, which reads for the averaged relative velocity $\langle v_r\rangle$

$$\eta=\frac{Ze^2}{4\pi\epsilon_0\hbar\langle v_r\rangle}=\frac{Z\alpha r_s}{(1+\Theta/2+(v/v_F)^2)^{1/2}}. \tag{12}$$

Here we approximated the mean electron velocity $\langle v_e\rangle$ by a simple interpolation between the Fermi velocity v_F and the thermal velocity $v_{th}=(k_BT/m)^{1/2}$ as $\langle v_e\rangle^2=v_F^2+v_{th}^2$ and $\langle v_r\rangle$ by $\langle v_r\rangle/v_F=(\langle v_e\rangle^2+v^2)^{1/2}/v_F=[1+\Theta/2+(v/v_F)^2]^{1/2}$, since $\Theta=2v_{th}^2/v_F^2$. The characterization of a weak perturbation by the assumption (10) in connection with condition (11) is confirmed by the behavior of the electron density ρ_{in} induced by the potential $\phi_p=Ze/4\pi\epsilon_0 r$ of an ion at rest $(v=0)$. A calculation of the induced density at position $r=0$, using the linear response relation $\tilde{\rho}_{in}(\mathbf{k})=Ze[1/\varepsilon(\mathbf{k},\omega=0)-1]$, yields $\rho_{in}(r=0)/\rho_0\propto\eta$, that is, the induced density is small compared to the unperturbed density $\rho_0=en$ for small η. Further, the linear regime of a small Bloch parameter coincides with the applicability of the first Born approximation for the ion-electron scattering, valid in the high energy regime $\eta\ll 1$. In fact, instead of deriving the stopping expression (4) from the induced electrical potential, it can be obtained alternatively from the energy and momentum transfer in ion-electron scattering events calculated in the first Born approximation for the *dynamically* screened potential of a cluster $\tilde{\phi}_c=\tilde{\rho}(\mathbf{k})/k^2\epsilon_0\varepsilon(\mathbf{k},\omega)$, that is, $\tilde{\phi}_p=Ze/k^2\epsilon_0\varepsilon(\mathbf{k},\omega)$ for a single ion (Born-RPA [22]). In particular, for parameters Z,n,T,v in agreement with Eqs. (11) and (12) the stopping has a pure quadratic dependence on the charge, as indicated in Eq. (6).

(*b*) *The semilinear regime*. Relations (11) and (12) demonstrate that the coupling always remains within the linear regime for sufficiently high projectile velocities v, while this is not the case at moderate velocities, in particular, for high charge states Z. A usual way to overcome the limitation of the dielectric formulation to the linear regime and, hence, to extend the linear response treatment to a larger set of parameters, is the restriction of the k integration in Eq. (4) through certain upper cutoffs k_m. Of course, at the expense of introducing some arbitrariness. The corresponding semilinear regime is characterized as follows. We reconsider the local condition for a weak perturbation (10) and look for a critical distance $r_c>0$, so that for $r>r_c$ [i.e., $V_{ei}(r_c)>V_{ei}(r)$] the local condition for a weak perturbation (10) holds, which defines r_c through

$$\varphi(r_c)=\tfrac{1}{2}. \tag{13}$$

The ion now represents a strong perturbation for $r<r_c$, a weak one for $r>r_c$ and, of course, no perturbation for r of

the order of λ_s and larger, where the ion potential is screened out completely. From this we establish the necessary condition

$$r_c \ll \lambda_s \tag{14}$$

for using a linear response description. Then, roughly speaking, the volume $\propto r_c^3$ where the perturbation is strong and its contribution to the stopping are very small compared to the whole interaction volume $\propto \lambda_s^3$ and the total stopping, respectively. We thus intend to exclude this small region of strong perturbation from the linear response treatment, while taking into account its small contribution, by introducing a suitably defined cutoff k_m in the k integration in Eq. (4), with $k_m \sim 1/r_c$.

To proceed, we turn to the binary collision treatment as an alternative approach to the stopping of single ions [23–27]. There the stopping arises from averaging binary collisions of the ion with not mutually interacting electrons, while the collective medium response is considered, in part, by replacing the pure Coulomb ion-electron interaction by a *statically* screened (Yukawa) potential, where the screening length is an external parameter. In the linear regime $\eta \ll 1$, the Born-RPA result (4) is, of course, superior to a first Born approximation in the binary collision model, since the Born RPA automatically accounts for the screening and, in addition, for the dynamic polarization processes (plasmon excitation). The binary collision approach yields identical results only in the limit of static response ($v \to 0$) when the corresponding static screening length is used and fits the Born RPA at high velocities $v \gg \langle v_e \rangle$, if one introduces the velocity dependent screening length $\lambda_s = v/\omega_p$. However, the binary collision description is not restricted to $\eta \ll 1$, and works, for known $\lambda_s(v)$, at all Coulomb parameters including the limit $\eta \gg 1$ of classical trajectories. Based on the expressions obtained in [24–28] the binary collision stopping power S_{bc} for any ion velocity v and degeneracy Θ can be approximated by

$$S_{bc} = Z^2 h(v) \left[\ln\left(\frac{2\lambda_s}{\lambda\!\!\!^{-}_r} \right) - \frac{1}{2} \ln(1+\gamma^2\eta^2) \right], \tag{15}$$

which approaches the exact results [26,27] in the limit $\lambda_s \gg b_0, \lambda\!\!\!^{-}_r$. Here $\lambda\!\!\!^{-}_r$ and η are defined as above, inserting the relative velocity $\langle v_r \rangle = (\langle v_e \rangle^2 + v^2)^{1/2}$, $\ln\gamma = 0.577\ldots$ is Euler's constant and $h(v)$ is a linear function in v for $v \ll \langle v_e \rangle$ and goes $\propto v^{-2}$ for $v \gg \langle v_e \rangle$. For its explicit form see, e.g., [27]. This result can now be compared to the stopping power S_{km}, obtained in the linear response formalism (4) (for $N=1$) when the k integration is restricted to $k \leqslant k_m$. S_{km} is of the same form as S_{bc} (15), i.e., a velocity dependent function times a logarithmic term and, ignoring some unimportant differences in the corresponding functions $h(v)$, the ratio of both stopping powers reads

$$\frac{S_{bc}}{S_{km}} \approx \frac{\ln(2\lambda_s) - \ln[\lambda\!\!\!^{-}_r (1+\gamma^2\eta^2)^{1/2}]}{\ln(k_m \lambda_s)}. \tag{16}$$

Here the velocity dependent effective screening length $\lambda_s(v)$ is taken from the linear response stopping power (4) with cutoff $k_m, S_{km} \propto \ln(k_m \lambda_s)$, where k_m is the external parameter and $\lambda_s(v)$ is provided by the dynamical response of the plasma due to the dielectric function. Subsequently, this effective screening length enters the binary collision treatment and the stopping power S_{bc}. Since screening has to obey certain constraints, e.g., complete screening of the projectile charge, such a procedure does not result in a consistent description in general, while it remains consistent within a first Born approximation as discussed in [29]. Here we focus only on the semilinear regime. There, the region of strong perturbation close to the projectile is per definition small compared to the region where the linear response (that is, first Born) is valid. Thus screening, which takes place at large impact parameters, is negligibly affected by the strong perturbation and remains close to the linear response behavior.

Comparison (16) now suggests the choice of the cutoff $k_m = 2/\lambda\!\!\!^{-}_r (1+\gamma^2\eta^2)^{1/2}$. Beyond the linear regime, for $\eta \gg 1 (b_0 \gg \lambda\!\!\!^{-}_r)$, we have $k_m = 2/\gamma\lambda\!\!\!^{-}_r \eta \approx 1/b_0$, whereas the definition of the critical distance r_c by Eqs. (10) and (13) [for $r_c \gg \lambda\!\!\!^{-}_r$ and $r_c \ll \lambda_s$ according to Eq. (14)] yields $2/r_c \approx 1/b_0$. In the linear regime $\eta \ll 1$ of the Born RPA no cutoff is needed at all, nevertheless, we can employ k_m as defined above, because now $k_m = 2/\lambda\!\!\!^{-}_r$ and it coincides with the cutoff originated from the behavior of the dielectric function and is intrinsic to the Born RPA. In any case, we have $b_o \ll \lambda_s$ and $\lambda\!\!\!^{-}_r = \alpha(3/2)^{1/2}(\xi(1+\Theta^2))^{1/2}/(v_r/v_F)^2\lambda_s < \xi^{1/2}\lambda_s \ll \lambda_s$ (for an ideal plasma $\xi \ll 1$), which are the preconditions for deriving expression (15).

In summary, we obtain from comparing with the binary collision approach, a recipe to determine k_m from η and r_c by defining

$$k_m = \begin{cases} \dfrac{2}{\lambda\!\!\!^{-}_r (1+\gamma^2\eta^2)^{1/2}}, & \eta \leqslant \frac{1}{2} \\ \dfrac{2}{\lambda\!\!\!^{-}_r [1+(\gamma/2)^2 + (r_c/\lambda\!\!\!^{-}_r)^2]^{1/2}}, & \eta > \frac{1}{2}. \end{cases} \tag{17}$$

As a consequence, the stopping power gets a logarithmic dependence on the charge in the semilinear regime in addition to the quadratic one. In a classical plasma ($\Theta \gg 1$) with Debye screening and $\eta \gg 1$, $r_c = 2b_0$, we recover in Eq. (17) the commonly used cutoff $k_m = 1/b_0$ and in the definition (14) of the semilinear regime ($r_c = 2b_0 \ll \lambda_s$) the weak coupling condition

$$\frac{2b_0}{\lambda_s} = \frac{Z}{2\pi n \lambda_D^3 [1+(v/v_{th})^2]^{3/2}} \ll 1, \tag{18}$$

where the ion charge state has to be small compared to the number of electrons in the dynamical screening sphere with $\lambda_s(v) = \lambda_D[1+(v/v_{th})^2]^{1/2}$ [30].

We will add some remarks to stress the content of the preceding consideration. Using the cutoff $k_m = 2/\lambda\!\!\!^{-}_r (1+\gamma^2\eta^2)^{1/2}$ in the dielectric linear response results in nothing else but a quantal-classical Bloch modification of stopping for $\eta \gg 1$ [23,24,26,27,31]. We do not only intend to reproduce this well-known form of the Bloch correction but also to establish the connection between the local strength of perturbation $\varphi(r)$ (10) and the cutoff parameter k_m as obtained in recipe (17), where $k_m = k_m(r_c)$ for

$\eta > 1/2$ with $\varphi(r_c) = 1/2$ [see Eq. (13)]. In Sec. II C 2 we use this relation to derive an approximation for the Bloch modification for the stopping of ion clusters. There, an exact calculation of the Bloch contribution to stopping is not easy to achieve, in general, since it requires the knowledge of the scattering phase shift for the complex scattering potential of an ion cluster including multiple scattering events. So far we only addressed the Bloch modification of stopping for semilinear ion-target coupling. There are also possible corrections due to a higher order target response, as contributions $\propto Z^3$ (Barkas) (see, e.g., [32,33]), which might compensate in certain situations, at least in part, the always negative Bloch term [31]. For the determination of the recipe to obtain the cutoff k_m for a single ion (17) or an ion cluster as given below, these higher order contributions are of no, or minor, importance, because they have to be added both to the linear response expression with cutoff S_{km} and the binary collision stopping power S_{bc}. The screening behavior should only be affected slightly, since higher order response contributions remain always small compared to the leading linear response term in the linear and semilinear regime. They may, however, alter the final results for the stopping power with respect to the linear response and Bloch terms only. The extension of the dielectric treatment of cluster stopping into the semilinear regime, discussed below, takes only into account the Bloch type correction related to small impact parameters. We assume that it is usually the more important correction, since strong coupling occurs only at small (compared to the screening length) distances. Nevertheless, further investigations are needed to determine the possible higher order polarization effects on ion cluster stopping for semilinear coupling.

To underline the significance of the semilinear regime for small clusters with high total charge, which are equivalent in their behavior to highly charged single ions, we show in Fig. 1 the target parameters (n,T) corresponding to the linear, semilinear, and nonlinear regime for an ion of charge state $Z=15$ and different relative velocities $\langle v_r \rangle$. The boundary which separates the linear regime at high temperatures and high densities from the semilinear one is indicated by the dashed curves for $\eta = 1/2$ given by definition (11) for $Z/\langle v_r \rangle = 15, 5, 1$ with $\langle v_r \rangle$ in units of $\langle v_e \rangle = (v_F^2 + v_{th}^2)^{1/2}$. For $Z=15$ this corresponds to an ion velocity small compared to the mean electron velocity $v \ll \langle v_e \rangle$, a medium velocity $v \lesssim 3\langle v_e \rangle$, and a high velocity $v \approx 15\langle v_e \rangle$, as well as to all other combinations of the same $Z/\langle v_r \rangle$ resulting in the same η [see Eq. (12)]. The dotted curves separate the semilinear from the nonlinear regime at low temperature and low densities employing the condition $b_0/\lambda_s = 1$, obtained by an approximative solution of Eq. (13) for $r_c \approx \lambda_s$ as an upper limit of r_c in definition (14), where $b_0/\lambda_s = 1$ is plotted for $Z=15$ and $\langle v_r \rangle = 1\ \langle v_e \rangle$ and $3\ \langle v_e \rangle$. The curve $\langle v_r \rangle = 15\ \langle v_e \rangle$ would already be outside the considered parameters. These curves also apply to other values of Z and $\langle v_r \rangle$ for the same $Z/\langle v_r \rangle^3 \propto b_0/\lambda_s$. Hence, Fig. 1 shows that the linear regime for highly charged ions or clusters at low velocities lies at extreme temperatures and densities, while the semilinear regime covers a much larger region and for modest velocities already the whole n,T region of interest for the given charge $Z=15$. For higher charges one stays even for large velocities within the semilinear region, while the linear one lies far beyond.

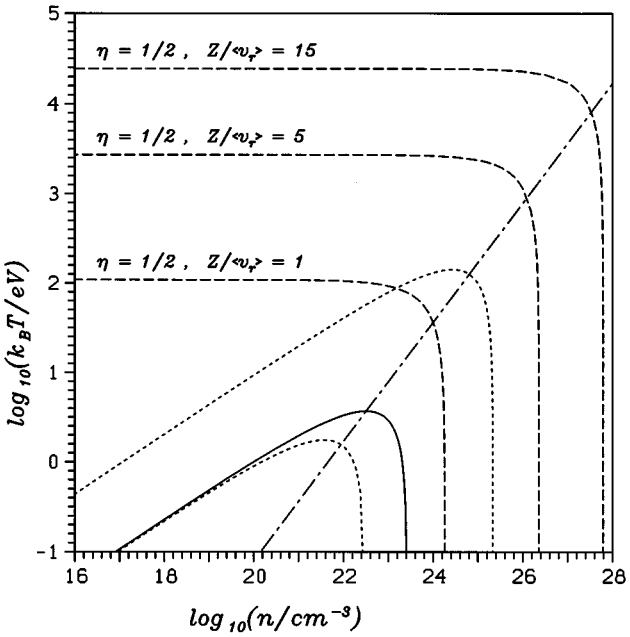

FIG. 1. The different regimes for the description of the energy loss of ions in an electron plasma of density n and temperature T. The dashed curves $\eta = 1/2$ separate the linear regime $\eta < 1/2$ at high temperatures and densities from the semilinear regime, which is located between the linear regime and the nonlinear regime boundary represented by the dotted curves $b_0/\lambda_s = 15$. From right top to left bottom, both dotted curves correspond to $Z/\langle v_r \rangle^3 = 15$ and 15/27, respectively, where $\langle v_r \rangle$ scales in $\langle v_e \rangle (n,T) = (v_F^2 + v_{th}^2)^{1/2}$. The nonideal targets are located below the solid curve $\xi = 1$, the degenerate targets below the dashed-dotted line $\Theta = 1$.

2. Weak coupling for ion clusters

For ion clusters things are much more involved, since the perturbing potential is the sum of the potentials of the cluster constituents and a comparison with a binary collision theory is not possible any more, except for the case of a pointlike cluster where the cluster size as a whole is small compared to $\lambda\!\!\!^{-}_r$. Hence, we propose to extend the above considerations for single ions to an appropriately defined cluster potential, in order to get the conditions for weak perturbation, as well as the cutoff required for a cluster in the semilinear regime.

We start with the potential energy for an electron in the field of the whole cluster V_{ce} as a superposition of the single ion expression V_{ei} given by Eq. (9), $V_{ce}(\mathbf{r}) = \Sigma_i V_{ei}(|\mathbf{r}_i - \mathbf{r}|)$, where we assumed for simplicity equal charges of the ions. As for a single ion, the strongest perturbation is caused at the ion location $\mathbf{r}_i$. In the cluster, the potential energy at the position of, for instance, the jth ion $V_{ce}(\mathbf{r} = \mathbf{r}_j)$ may, however, exceed the single ion value at the origin $V_{ei}(r=0)$ due to the vicinity of the other $(N-1)$ ions. For measuring the strength of the perturbation it is thus reasonable to choose the position of an ion in the cluster as the origin and to perform subsequently an average over the N possibilities. This establishes the following mean potential energy for an electron in the field of the cluster:

$$\langle V(\mathbf{r})\rangle = \frac{1}{N}\sum_i \sum_j V_{ei}(|\mathbf{r}_i-\mathbf{r}_j-\mathbf{r}|)$$

$$= V_{ei}(r) + \frac{1}{N}\sum_i \sum_{j\neq i} V_{ei}(|\mathbf{r}_i-\mathbf{r}_j-\mathbf{r}|). \quad (19)$$

However, to provide a useful tool to determine the quantities of interest, some further averages on $\langle V(\mathbf{r})\rangle$, at least an angular one, are still necessary. If we are interested again in the common features of correlated stopping rather than in the properties of a single, selected cluster, an average over an ensemble of clusters, as described above for deriving the mean stopping power (6), results in an averaged expression $\langle\langle V\rangle\rangle$ which reads with the help of the pair-distribution function $g(|\mathbf{r}_i-\mathbf{r}_j|)$ (assuming a spherical cluster)

$$\langle\langle V(r)\rangle\rangle = V_{ei}(r) + \int d^3\tilde{r}\; V_{ei}(|\tilde{\mathbf{r}}-\mathbf{r}|)g(\tilde{r}). \quad (20)$$

This averaged quantity $\langle\langle V(r)\rangle\rangle$ now allows us to define the linear and semilinear regime and the parameter r_c in a manner analogous to the single ion case considered above. By introducing the quantity φ_c, the definitions (10) and (13) are altered to

$$\varphi_c(r) = \frac{\langle\langle V(r)\rangle\rangle}{mv_r^2} \leqslant \frac{1}{2}, \quad \varphi_c(r_c) = \tfrac{1}{2}. \quad (21)$$

Keeping in mind that $\varphi(0)=\eta$ [Eq. (11)] for a single ion, we suggest as an extension of the single ion case (17) to ion clusters the choice of a cutoff for clusters

$$k_m^c = \begin{cases} \dfrac{2}{\lambda\!\!\!^{-}_r[1+\gamma^2\varphi_c^2(0)]^{1/2}}, & \varphi_c(0)\leqslant\frac{1}{2} \\ \dfrac{2}{\lambda\!\!\!^{-}_r[1+(\gamma/2)^2+(r_c/\lambda\!\!\!^{-}_r)^2]^{1/2}}, & \varphi_c(0)>\frac{1}{2}, \end{cases} \quad (22)$$

with $\varphi_c(0)$ and r_c from Eq. (21). Except for the linear Born-RPA regime $1/2>N\eta=N\varphi(0)=\max(\varphi_c(r))$, where $k_m^c\approx 2/\lambda\!\!\!^{-}_r$, the delicate interplay of cluster and target parameters requires a detailed study of φ_c and k_m^c for the ion clusters of interest. We resume these investigations for the examples discussed below.

D. Some provisional conclusions and definitions

We conclude this section on the description of the stopping of ion clusters by summarizing some general features contained in the stopping formulas (4) and (6). In the pure linear regime $[\varphi_c(0)\ll 1]$, the linearity and the connected superposition principle allow the correlated part of the stopping to be entirely built up by two ion pair contributions, where each pair already exhibits every basic feature of correlated stopping. This can be expressed by reformulating Eq. (4) as a contribution of single isolated ions and a correlation part C, which is the sum of binary contributions

$$S = \sum_n Z_n^2 S_1 + C = \sum_n Z_n^2 S_1 + \sum_n \sum_{m\neq n} Z_n Z_m C_2(\mathbf{r}_{nm}), \quad (23)$$

where $\mathbf{r}_{nm}=\mathbf{r}_n-\mathbf{r}_m$, S_1 the single ion stopping $S_1=C_2(\mathbf{r}_{nm}=0)$, and C_2 the pair correlation function

$$C_2(\mathbf{r}) = \frac{e^2}{\epsilon_0(2\pi)^3}\int d^3k \frac{\mathbf{k}\cdot\hat{\mathbf{v}}}{k^2}\,\mathrm{Im}\left[\frac{-1}{\varepsilon(\mathbf{k},\mathbf{k}\cdot\mathbf{v})}\right]\exp(i\mathbf{k}\cdot\mathbf{r}), \quad (24)$$

which depends only on the components of $\mathbf{r}$ parallel and perpendicular to the velocity $\mathbf{v}$. This emphasizes the importance of the detailed studies of ion pairs [1,3,8,9,34] and simple structures built up on a few pairs [6,10]. To quantify the effects of correlations on the cluster stopping we define the enhancement factor ϵ as the total cluster stopping S, with respect to the isolated particle stopping $\Sigma_n Z_n^2 S_1$

$$\epsilon = \frac{S}{\Sigma_n Z_n^2 S_1} = 1 + \frac{C}{\Sigma_n Z_n^2 S_1}. \quad (25)$$

As a boundary for the binary correlation C_2 we have $|C_2|\leqslant|S_1|$ and $|C/S_1|\leqslant(\Sigma_n Z_n)^2-\Sigma_n Z_n^2$ from the definition above. Because the total stopping S (4) and (6) is of the same sign as S_1, we get

$$0 \leqslant \epsilon \leqslant \frac{\left(\sum_n Z_n\right)^2}{\sum_n Z_n^2}, \quad (26)$$

with $\epsilon<1$ belonging to the case of a reduction of stopping by correlations while the upper limits represent the complete coalescence of the clusters. For clusters of equal charges this simplifies to $0\leqslant\epsilon\leqslant N$. These definitions and ratios are independent of the plasma parameters and apply to hot classical plasmas as well as to electron jellium ($T=0$) provided that the coupling remains within the linear regime. In the semilinear regime the functions C_2 depend on the whole cluster structure via the cutoff k_m^c (i.e., r_c). The stopping of the cluster cannot be constructed only by calculating and summing up the pair correlations $C_2(\mathbf{r}_{nm})$ for the relative positions $\mathbf{r}_n-\mathbf{r}_m$. Now, the knowledge on the total distribution of the ions $\{\mathbf{r}_i\}$ is required and Eq. (23) is replaced by $S=\Sigma_n Z_n^2 S_1^c+\Sigma_n\Sigma_{m\neq n} Z_n Z_m C_2^c(\mathbf{r}_{nm})$, where the subscript c denotes this dependence on the whole structure. That is, Eq. (24) changes to

$$C_2^c(\mathbf{r}) = \frac{e^2}{\epsilon_0(2\pi)^3}\int_{|\mathbf{k}|\leqslant k_m^c} d^3k \frac{\mathbf{k}\cdot\hat{\mathbf{v}}}{k^2}\,\mathrm{Im}\left[\frac{-1}{\varepsilon(\mathbf{k},\mathbf{k}\cdot\mathbf{v})}\right]\exp(i\mathbf{k}\cdot\mathbf{r}), \quad (27)$$

and $S_1^c=C_2^c(\mathbf{r}_{nm}=0)$. The boundaries given in Eq. (26) remain valid. However, one usually cannot expect the upper one for complete coalescence. In this limit, ϵ/N, the enhancement divided by N for a cluster of N ions with charge Z, is just the ratio of the stopping power of a single ion with charge NZ to N^2 times those of a single ion with charge Z. This quantity is shown in Fig. 2, as function of the velocity v and for different N,Z and parameters of the target plasma using the cutoff k_m and k_m^c determined by the definitions (17) and (13) and (22) and (21) with $\varphi_c(r)=N\varphi(r)$. The additional dependence of the stopping power on the charge in the

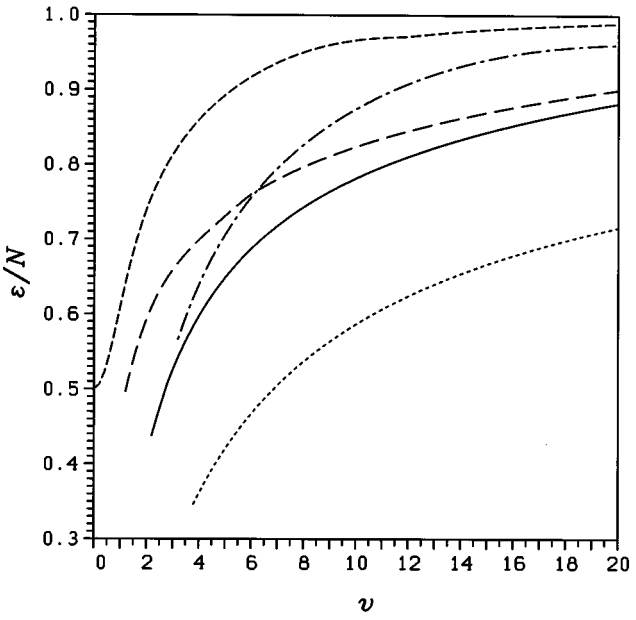

FIG. 2. Enhancement ϵ/N for a cluster of N ions with charge state Z in the case of complete coalescence and for different target densities n and temperatures T as a function of the cluster velocity v scaled in units of $\langle v_e\rangle(n,T)=(v_F^2+v_{th}^2)^{1/2}$. For an electron jellium $(T=0)$ with $n=1.61\times10^{24}$ cm^{-3} $(r_s=1)$ and $Z=1$, $N=20$ (dashed-dotted curve) and classical plasmas with $T=12$ eV, $n=4\times10^{20}$ cm^{-3}, $Z=1$, $N=20$ (solid), $Z=1$, $N=100$ (dotted), and $T=300$ eV, $n=10^{22}$ cm^{-3}, $Z=1$, $N=20$ (short-dashed), $Z=10$, $N=10$ (long-dashed). The curves are truncated when the nonlinearity becomes too strong for the present description to be valid.

semilinear regime results in a considerable lower enhancement in a wide range of target condition, in particular, for high charges NZ and modest velocities. For high velocities the semilinear regime merges into the linear regime and $\epsilon\to N$, while for small v the nonlinear regime may be reached if $r_c\to\lambda_s$ according to condition (14). For cases in Fig. 2 where this happens the corresponding curves are truncated at $r_c>0.25\lambda_s$.

For an ion cluster with finite size, results on the enhancement in the semilinear regime will be given in Sec. III.

III. RESULTS FOR SOME GENERIC EXAMPLES

A. Spherical ion clouds of Gaussian shape

As a first example we study the stopping of a spherical ion cloud, where the ions are distributed independently of each other around the center of the cluster with a Gaussian probability density resulting in

$$g(r)=(N-1)\left(\frac{1}{4\pi\sigma^2}\right)^{3/2}\exp\left(-\frac{r^2}{4\sigma^2}\right),$$

$$\Sigma(\mathbf{k})=1+(N-1)\exp(-k^2\sigma^2), \tag{28}$$

with the distance between two ions r and the rms radius σ as a measure for the cluster size. This ion configuration allows for a relatively easy mathematical treatment, but, nevertheless, represents a rather useful model to investigate the behavior of ion debris of various ion distributions produced in the fragmentation process of the cluster ions when impacting the plasma.

Rewriting Eq. (6) by setting $\mathbf{k}\cdot\mathbf{v}=\omega$, the ensemble averaged stopping power per ion for the Gaussian cluster takes the form

$$\begin{aligned}\frac{\langle S\rangle}{N}&=\frac{Z^2e^2}{v^2 2\pi^2\epsilon_0}\int_0^{k_m^c}\frac{dk}{k}\int_0^{kv}d\omega\,\omega\,\mathrm{Im}\left[\frac{1}{\varepsilon(k,\omega)}\right]\\&\quad+(N-1)\frac{Z^2e^2}{v^2 2\pi^2\epsilon_0}\int_0^{k_m^c}dk\,\frac{\exp(-k^2\sigma^2)}{k}\\&\quad\times\int_0^{kv}d\omega\,\omega\,\mathrm{Im}\left[\frac{1}{\varepsilon(k,\omega)}\right]\\&=Z^2S_1^c+(N-1)Z^2C_2^c,\end{aligned} \tag{29}$$

where S_1^c, C^c in the semilinear regime depend on the whole cluster structure via the cutoff k_m^c; see Eqs. (20)–(22). Then, S_1^c represents a single particle stopping contribution in the presence of the cluster and is in general not identical to the stopping power S_1 of an isolated ion of the same charge state. In the linear (Born) regime such a cutoff is not required, but coincides with the intrinsic cutoff of $\mathrm{Im}[1/\varepsilon(k,\omega)]$ and $S_1^c=S_1$. The correlation part C_2^c is the averaged pair correlation function Eq. (27) as well as the total correlation part of stopping divided by $N(N-1)$. We mainly focus the discussion of correlated stopping of the Gaussian cluster on the enhancement ϵ, which now reads

$$\epsilon=\frac{\langle S\rangle}{NZ^2S_1}=\frac{S_1^c}{S_1}+(N-1)\frac{C_2^c}{S_1}. \tag{30}$$

In the limits of large velocities $v\gg\langle v\rangle$ (any degeneracy) and for low velocities for highly degenerate $\Theta\ll1$ and classical plasma $\Theta\gg1$, an analytical evaluation of the stopping power given by Eq. (29) with the RPA dielectric function [17,22] is possible. By an interpolation between these analytical expressions we derived a formula for the enhancement ϵ at all v and Θ, which agrees well with the numerical solutions for $\langle S\rangle/(NZ^2S_1)$ and allows for a fast calculation of the enhancement. This interpolation formula is expressed in terms of a function ζ, which is connected to the enhancement for the Gaussian cluster by

$$\epsilon=\frac{\zeta(v,0,k_m^c)}{\zeta(v,0,k_m)}+(N-1)\frac{\zeta(v,\sigma,k_m^c)}{\zeta(v,0,k_m)}, \tag{31}$$

and where ζ is defined as

$$\begin{aligned}\zeta(v,\sigma,\kappa)&=\frac{\beta^2\exp(-\sigma^2\delta^2)}{\beta^2+\delta^2}-1-(1+\sigma^2\beta^2)\exp(\sigma^2\beta^2)\\&\quad\times[E_1(\sigma^2(\beta^2+\delta^2))-E_1(\sigma^2\beta^2)]\\&\quad+E_1(\sigma^2\delta^2)-E_1(\sigma^2\kappa^2),\end{aligned} \tag{32}$$

with the exponential integral $E_1(z)=\int_z^\infty\exp(-t)/t\,dt$ and the coefficients β,δ adapted to fit the exact solution in the known limits

$$\beta^2=\frac{3+\frac{3}{2}\Theta+0.408v^2\left(\frac{3.819}{0.408}+\frac{3}{2}\Theta\right)}{(1+\frac{3}{2}\Theta)(1+v^2)},\quad \delta=\frac{\kappa(1+v^2)}{1+\kappa v^3}. \tag{33}$$

Here v is scaled in units of the mean electron velocity $\langle v_e\rangle=v_F(1+\Theta/2)^{1/2}$, σ in units of λ_0 and κ in $1/\lambda_0$, with the static screening length $\lambda_0=\langle v_e\rangle/\omega_p$. This scaling behavior of ζ and, hence, of enhancement ϵ, assigns an important role to the ratios σ/λ_0 and $v/\langle v_e\rangle$ as decisive parameters to characterize correlated stopping.

The cutoffs k_m and k_m^c entering the function ζ are given by definition (17) for k_m and by evaluating Eqs. (20)–(22) for the Gaussian cluster to obtain k_m^c. Inserting $g(r)$ Eq. (28) in Eq. (20) yields r_c as the solution of $\varphi_c(r_c)=1/2$, where $\varphi_c(r)$ has the explicit form

$$\varphi_c(r)=\varphi(r)+\frac{N-1}{2}\frac{b_0}{r}\left[\Lambda_\sigma\left(r,\frac{1}{\lambda_s}\right)-\Lambda_\sigma\left(r,\frac{1}{\lambda_r}+\frac{1}{\lambda_s}\right)\right], \tag{34}$$

with the single ion expression (10) as defined in the preceding section, the dynamical screening length $\lambda_s=v_r/\omega_p=\lambda_0(1+v^2)^{1/2}$ and

$$\Lambda_\sigma\left(r,\frac{1}{\lambda}\right)=\exp\left(\frac{\sigma^2}{\lambda^2}\right)\left[\exp\left(-\frac{r}{\lambda}\right)\operatorname{erfc}\left(-\frac{r}{2\sigma}+\frac{\sigma}{\lambda}\right)-\exp\left(\frac{r}{\lambda}\right)\operatorname{erfc}\left(\frac{r}{2\sigma}+\frac{\sigma}{\lambda}\right)\right]. \tag{35}$$

Here erfc is the complementary error function $\operatorname{erfc}(z)=2/\sqrt{\pi}\int_z^\infty\exp(-t^2)dt$.

The resulting influence on the stopping, respectively, the enhancement, due to the dependence of the cutoffs k_m^c, k_m on the cluster and ion parameters N, σ, Z, and v will be discussed later. For the moment we set the cutoffs to $k_m^c=k_m=2/\lambda_r$. For this setting, Fig. 3 shows the enhancement ϵ as function of the cluster size σ obtained by Eqs. (31)–(33) (curves) compared to the exact numerical solutions of Eq. (29) (crosses) for a cluster of $N=10$ ions for different velocities v and two sets of target parameters, corresponding to an electron jellium and a classical plasma. The agreement of formula (31) with the exact result is almost perfect for high and low velocities where it was fitted to the analytic results and displays deviations of some percent for intermediate velocities. The presented expression (31) thus allows rather accurate and fast calculation, and can be used in future work to include the, so far, neglected Coulomb explosion into the description of the cluster slowing down by replacing the cluster size σ by a time dependent one $\sigma(t)$. Using a simple model for the explosion $\sigma(t)$, such a procedure yields a fast and valuable overview on the effects of the Coulomb explosion for the various target and cluster conditions of interest, which is hardly achievable with very expensive full calculations. In addition, Eqs. (31)–(33) are much more suitable for a good understanding of the basic aspects of correlated stopping and the physics behind it than original expression Eq. (29). Inspecting Eqs. (31)–(33), for this purpose, more closely, we first recall the behavior of the exponential integral $E_1(z)$ for small and large arguments ($\ln\gamma=0.577\ldots$)

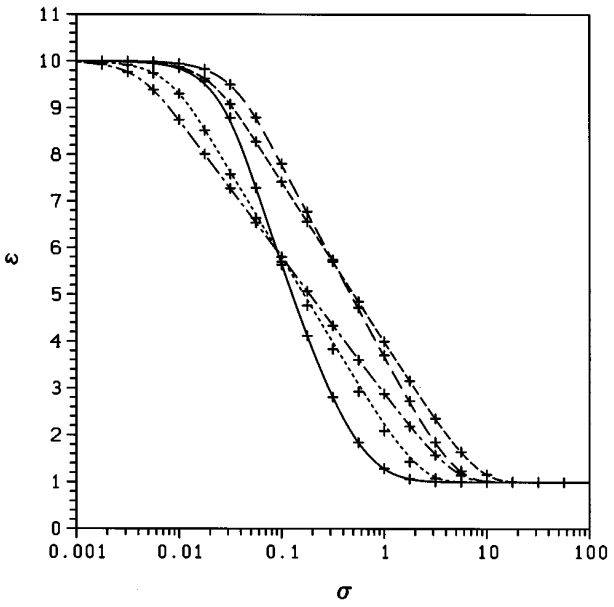

FIG. 3. Enhancement ϵ for a Gaussian cluster of $N=10$ ions with charge state $Z=1$ as function of the cluster size σ in units of the screening length $\lambda_0(n,T)=\langle v_e\rangle/\omega_p=(v_F^2+v_{th}^2)^{1/2}/\omega_p$. The curves show the results of the presented interpolation formula and the crosses the corresponding exact numerical evaluations for a jellium ($T=0$) with $n=1.61\times10^{24}$ cm^{-3} ($r_s=1$) and cluster velocities $v/\langle v_e\rangle=v/v_F=6$ (long-dashed curve) and 10 (short-dashed) and for a classical plasma with $T=12$ eV, $n=4\times10^{20}$ cm^{-3} for $v/\langle v_e\rangle=v/v_{th}=0.1$ (solid), 3 (dotted), and 6 (dashed-dotted).

$$E_1(z)\sim\begin{cases}-\ln(z)-\ln\gamma+O(z), & z\ll1\\ \dfrac{\exp(-z)}{z}\left[1-\dfrac{1}{z}+\dfrac{2}{z^2}+O\left(\dfrac{1}{z^3}\right)\right], & z\gg1,\end{cases} \tag{36}$$

from which we obtain ζ in the special case of complete coalescence $\sigma=0$ as

$$\zeta(v,0,\kappa)=\frac{\beta^2}{\beta^2+\delta^2}-1+\ln\left(\frac{\kappa^2(\beta^2+\delta^2)}{\beta^2\delta^2}\right) \tag{37}$$

resulting in the enhancement $\epsilon(\sigma=0)$ already presented in Fig. 2

$$\epsilon(\sigma=0)=N\frac{\zeta(v,0,k_m^c)}{\zeta(v,0,k_m)}\approx N\begin{cases}\dfrac{\ln[(k_m^c/\beta)^2+1]-1}{\ln[(k_m/\beta)^2+1]-1}, & v\ll1\\ \dfrac{\ln(vk_m^c)}{\ln(vk_m)}, & v\gg1,\end{cases} \tag{38}$$

where we used $k_m^c/\beta, k_m/\beta\gg1$ and $vk_m^c, vk_m\gg1$, respectively, valid for the considered linear and semilinear regimes.

For the general case of arbitrary σ the different values of β, δ, and κ are directly related to three different correlation regimes.

1. Short range correlations: Complete coalescence

For $\sigma k_m^c\ll1$, which implies also $\sigma\beta,\sigma\delta\ll1$, because $\beta(v,\Theta)\sim1$, $\delta\lesssim k_m^c$, and $k_m^c\gg1$, all exponential integrals

in ζ can be expressed asymptotically for small arguments through $E_1(z)\sim-\ln(z)-\ln\gamma$. This results in $\zeta(v,\sigma,k_m^c \ll 1/\sigma)\sim\zeta(v,0,k_m^c)$ given by Eq. (37) and $\epsilon\sim\epsilon(\sigma=0)$ Eq. (38). The physical origin for this behavior is obvious from the definition of k_m^c, where we have $\sigma\ll 1/k_m^c\approx\lambda\!\!\!^{-}_r$ in the linear regime and $\sigma\ll 1/k_m^c\approx r_c$ in the semilinear regime, respectively. While in the linear regime the cluster is smaller than the electron wavelength and thus appears as pointlike, the radius $r_c\sim b_0$ remains smaller than the distance of closest approach of the classical trajectories for most of the electrons in the semilinear case. This is consistent with the form of the cluster potential φ_c (34) evaluated in the two corresponding limits of small σ

$$\varphi_c(r)=\begin{cases}\dfrac{Nb_0}{r}\left[1-\exp\left(-\dfrac{r}{\lambda\!\!\!^{-}_r}\right)\right] & \text{for}\quad \sigma\ll\lambda\!\!\!^{-}_r,\ r\approx\lambda\!\!\!^{-}_r\ll\lambda_s\\ \dfrac{Nb_0}{r}\exp\left(-\dfrac{r}{\lambda_s}\right) & \text{for}\quad \sigma\ll r_c,\ r\approx r_c\gg\lambda\!\!\!^{-}_r.\end{cases} \tag{39}$$

2. Long range correlations: Single ion stopping

In the limit $\sigma k_m^c,\sigma\beta,\sigma\delta\gg 1$, that is, cluster large compared to the screening length $\sigma\gg\lambda_s\approx\max(1/\beta,1/\delta)\approx(1/\beta^2+v^2)^{1/2}$ (in the used scaling), the contribution of the correlation part to the stopping vanishes like

$$\zeta[v,\sigma\gg\max(1/\beta,1/\delta),k_m^c\gg 1/\sigma]\sim\frac{1}{\sigma^4\beta^4}-\frac{\exp(-\sigma^2\delta^2)}{\sigma^2(\beta^2+\delta^2)}\times\left(1-\frac{\beta^2}{\beta^2+\delta^2}\right) \tag{40}$$

and behaves for large σ as $1/\sigma^4$. This qualitative behavior can also be deduced simply from the original expression for the stopping (6) with the structure factor (28). For the present Gaussian cluster without any further structure the limit of long range correlations is just the limit of isolated ions.

3. Intermediate range regime

When the cluster is not pointlike, that is, $\sigma k_m^c\gg 1$, but smaller than the screening length, $\sigma\ll\max(1/\beta,1/\delta)$, the enhancement shows a logarithmic increase with decreasing cluster size σ, where ζ can be approximated as

$$\zeta(v,\sigma,k_m^c\gg 1/\sigma)\sim\begin{cases}\dfrac{\beta^2}{\beta^2+\delta^2}-1-\ln\gamma-\ln\left(\dfrac{\sigma^2\beta^2\delta^2}{\beta^2+\delta^2}\right), & \sigma\beta,\sigma\delta\ll 1\\ -1-\ln\gamma-\ln(\sigma^2\beta^2), & \sigma\beta\ll 1,\sigma\delta\gg 1\\ -\ln\gamma-\ln(\sigma^2\delta^2), & \sigma\beta\gg 1,\sigma\delta\ll 1.\end{cases} \tag{41}$$

In summary, we have for a given velocity v a dependence of the enhancement ϵ on a growing cluster size σ, which is characterized by a constant value for small clusters $\sigma\ll 1/k_m^c$, by a change to a logarithmic decrease starting at $\sigma\approx k_m^c$ and persisting until σ reaches the (dynamical) screening length. Finally one approaches the isolated, single ion limit $\epsilon\to 1$ for larger σ. Because k_m^c and the dynamical screening length λ_s are increasing functions for increasing cluster velocities, the boundaries of the logarithmic dependence on σ are extended to smaller σ via k_m^c at one end of the scale and to larger σ via λ_s at the other one. This velocity dependence as well as the dependence of the target conditions on the transition to the regime of complete coalescence is nicely pictured by the various cases of Fig. 3, where σ is given on a logarithmical scale.

In this context, it is also of interest to have a look at the case of large velocities v for a cluster with fixed size σ. In particular, we regard the conditions $v\gg 1$ (in units of $\langle v_e\rangle$) and a velocity which is sufficiently high so that the cluster is both non-point-like ($\sigma k_m^c\gg 1$) and small compared to the dynamical screening length λ_s, that is in the dimensionless quantities $\sigma\ll v$. Because $\delta\sim 1/v$ and thus $\sigma\delta\ll 1$, $\delta\ll\beta$, we have $\zeta(v,\sigma,k_m^c)\sim-\ln\gamma-\ln(\sigma^2/v^2)$ while $\zeta(v,0,\kappa=k_m^c,k_m)\sim 2\ln(\kappa v)$. This results in the enhancement

$$\epsilon=\frac{\ln(vk_m^c)}{\ln(vk_m)}+(N-1)\frac{-\ln\gamma+\ln(v^2/\sigma^2)}{2\ln(vk_m)}\sim 1+(N-1)\frac{\ln(v)}{\ln(v^2)}=\frac{N+1}{2}, \tag{42}$$

where the terms to the right represent the limit $v\to\infty$, hence $\ln(v)\to\infty$ and $k_m^c\to k_m\to 2\lambda_0/\lambda\!\!\!^{-}_r\propto v$. The result $\epsilon(v\to\infty)\to(N+1)/2$ has to be considered mainly as a mathematical one, because we deal with a description of correlated stopping, which is restricted to nonrelativistic velocities. Depending on the given parameters of the cluster and the target this limit may, however, be reached already for nonrelativistic velocities and has the following physical meaning. As known, the stopping of a single ion at high velocities is to one half due to single particle excitations and to the other half to collective excitations of plasma waves. The wavelength λ_p of the plasmons excited with the phase velocity v is $\lambda_p=2\pi v/\omega_p$, that is, in scaled values $\lambda_p=2\pi v$. For this plasma waves with $\lambda_p\gg\sigma$ the cluster appears as pointlike and the stopping of the cluster by collective excitations is the same as the stopping by collective excitations of a single ion with the total charge NZ. The single particle excitations resolve the cluster structure

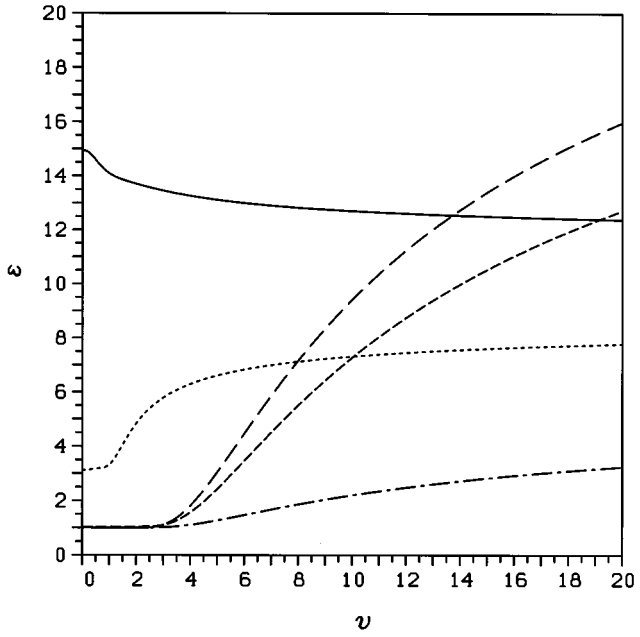

FIG. 4. Enhancement ϵ for a Gaussian cluster of ions with $Z=1$ as a function of the cluster velocity v in units of $\langle v_e\rangle=(v_F^2+v_{th}^2)^{1/2}$. For a target plasma $T=12$ eV, $n=4\times10^{20}$ cm^{-3} and clusters with $N=20$ ions and a size $\sigma=0.05$ (solid curve), 0.5 (dotted), 5 (dashed-dotted). For clusters of $N=100$, $\sigma=5$ with the same target conditions (short-dashed) and for a jellium target $T=0$, $n=1.61\times10^{24}$ cm^{-3} $(r_s=1)$ (long-dashed curve). The cluster sizes σ are in units of the screening length $\lambda_0(n,T)=\langle v_e\rangle/\omega_p$.

and correspond to N times the single particle contribution for single ions with charge Z. This yields in summary an enhancement $\epsilon=\langle S\rangle/NZ^2S_1=[(NZ)^2/2+NZ^2/2]/NZ^2=(N+1)/2$. The velocity dependence of the enhancement is shown in Fig. 4 for different cluster sizes σ, numbers N of ions and target parameters, again for the setting $k_m^c=k_m=2/\lambda\!\!\!^{-}_r$ as in Fig. 3. While the trend is visible, the high velocity limit $(N+1)/2$ still lies far away for the given velocity range and parameters. It can be reached only through the weak logarithmic v dependence of ϵ, given by Eq. (42). For high numbers of ions and cluster sizes of the order of the dynamical screening length a considerable enhancement arises at high velocities. It remains, nevertheless, small compared to the achievable limit $\epsilon\sim N/2$. Such increases of correlated stopping for high velocities have be documented also for other cluster configurations [5,35] with comparable values of the cluster size with respect to the screening length.

To investigate the behavior of enhancement including the semilinear regime the corresponding cutoffs $k_m^c=k_m^c(N,Z,v,\sigma)$ and $k_m=k_m(Z,v)$ have to be determined following the procedures developed in the preceding section and then included in the expressions for the enhancement. This will change the maximal achievable enhancement, as already demonstrated, and, in particular, the dependence on the ion number N. However, for a lot of cases one remains within the linear regime, namely, for large or weakly charged clusters and at high velocities. There the N dependence is purely linear for a given σ as suggested by the definitions (29)–(31).

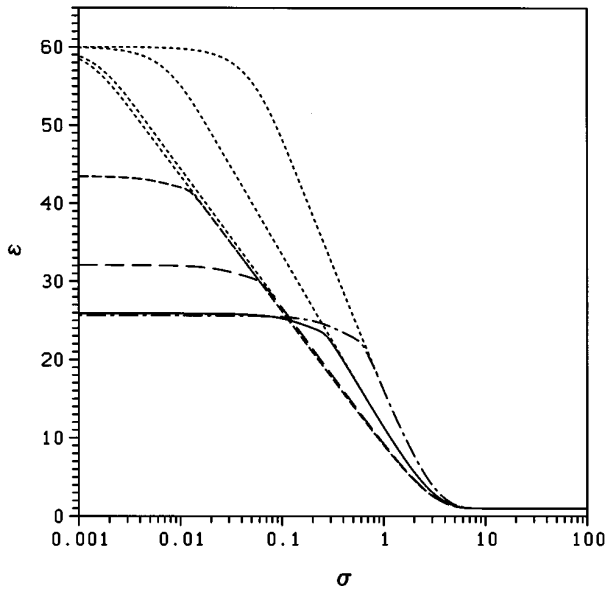

FIG. 5. Enhancement ϵ for a Gaussian cluster of $N=60$ ions and velocity $v/\langle v_e\rangle=4$ as a function of the cluster size σ in units of $\lambda_0(n,T)=\langle v_e\rangle/\omega_p=(v_F^2+v_{th}^2)^{1/2}/\omega_p$. For plasmas with $T=12$ eV, $n=4\times10^{20}$ cm^{-3} and ions with charge state $Z=1$ (solid curve), $T=0$, $n=1.61\times10^{24}$ cm^{-3}, $Z=1$ (dashed-dotted), $T=300$ eV, $n=10^{22}$ cm^{-3}, $Z=1$ (short-dashed) and $Z=5$ (long-dashed). In each case, the dotted curves exhibit the enhancement for a pure linear behavior of the stopping when nonlinear effects which appear in the semilinear regime are neglected.

The enhancement obtained by taking the nonlinear effects contained in k_m^c into account is shown in Figs. 5 and 6 for a cluster of $N=60$ ions at velocities $v=4$ and 10 for various target conditions and ion charges Z. The enhancement exhibits the typical logarithmic increase for decreasing σ starting when the cluster size becomes smaller than the dynamical

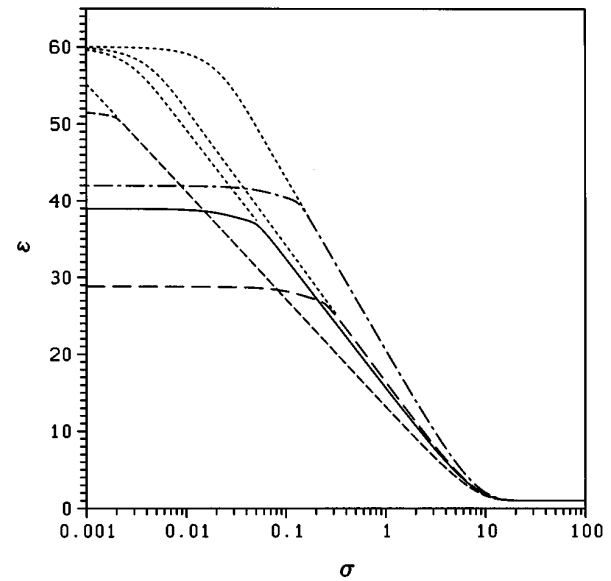

FIG. 6. Enhancement ϵ for a Gaussian cluster of $N=60$ ions as in Fig. 5 but now for a velocity $v/\langle v_e\rangle=10$ and for $T=12$ eV, $n=4\times10^{20}$ cm^{-3}, $Z=1$ (solid curve) and $Z=5$ (long-dashed), $T=0$, $n=1.61\times10^{24}$ cm^{-3}, $Z=1$ (dashed-dotted) and $T=300$ eV, $n=10^{22}$ cm^{-3}, $Z=1$ (short-dashed).

screening length which grows with velocity. This increase stops at a certain cluster size and approaches a constant value of maximal enhancement, which lies, for most of the presented cases, well below the *a priori* limit $\epsilon = N$ reached by the dotted curves, which are obtained by ignoring the effect of an increasing perturbation on the target for decreasing σ and setting $k_m^c = k_m$, which is independent on σ. At the point where the enhancement reaches this constant value, the shrinking cluster is no longer a weak enough perturbation to remain within the linear regime. The behavior of the enhancement is thus monitored by the additional dependence on the cluster charge and reaches for a further decrease of the size σ the maximal achievable enhancement in the semilinear regime. This reduction of the enhancement is significant even at relatively high cluster velocities and will become more and more important for higher charge states and numbers of ions.

To improve the simple model of the Gaussian ion distribution, an additional (internal) structure can be introduced, which accounts for the spacing between the ions as one expects for real ion debris, as a consequence of the initial arrangement before fragmentation and of the mutual repulsion during the slowing down. Intending to take this into account, in quite a general manner, as well as to benefit from the efforts for the description of the Gaussian cluster, we again employ a Gaussian profile for modeling this internal structure by

$$g(r) = \frac{N-1}{\chi^{3/2}-1}\left(\frac{\chi}{4\pi\sigma^2}\right)^{3/2} \exp\left(-\frac{r^2}{4\sigma^2}\right)\left[1-\exp\left(-\frac{r^2}{4\varsigma^2}\right)\right],$$

$$\chi = 1 + \frac{\sigma^2}{\varsigma^2}. \tag{43}$$

Here σ is again the measure for the cluster size as a whole, while ς defines a typical interion spacing. In contradiction of the preceding model without internal structure, the probability in the improved model to find two ions at the same position, is zero and strongly reduced for mutual distances $r \leqslant \varsigma$. Because the volume occupied by one ion is of the order ς^3, while the whole cluster has a volume of about σ^3, $\sigma^3/\varsigma^3 \approx N$. For further simplification we chose $\sigma^2/\varsigma^2 = N^{2/3} - 1$ in order to get $\chi^{3/2} = (1+\sigma^2/\varsigma^2)^{3/2} = N$. With this choice the structure factor has the simple form

$$\Sigma(\mathbf{k}) = 1 + N\left\{\exp(-k^2\sigma^2) - \frac{1}{N}\exp\left[-k^2\left(\frac{\sigma}{N^{1/3}}\right)^2\right]\right\}, \tag{44}$$

while the corresponding enhancement reads

$$\epsilon_\varsigma = \frac{\zeta(v,0,k_m^c)}{\zeta(v,0,k_m)} + N\frac{\zeta(v,\sigma,k_m^c)}{\zeta(v,0,k_m)} - \frac{\zeta(v,\sigma/N^{1/3},k_m^c)}{\zeta(v,0,k_m)}, \tag{45}$$

with ζ from Eq. (32). In an analogous manner, expression (34) for $\varphi_c(r)$ has to be modified using the functions Λ_σ and $\Lambda_{\sigma/N^{1/3}}$ to obtain the corresponding values for r_c and k_m^c. To investigate the additional effects, we regard the relative deviations between both enhancements ϵ_ς and ϵ with and without internal structure given by

$$\triangle\epsilon = \frac{\epsilon_\varsigma - \epsilon}{\epsilon} = \frac{-\zeta(v,\sigma/N^{1/3},k_m^c) + \zeta(v,\sigma,k_m^c)}{\zeta(v,0,k_m^c) + (N-1)\zeta(v,\sigma,k_m^c)}. \tag{46}$$

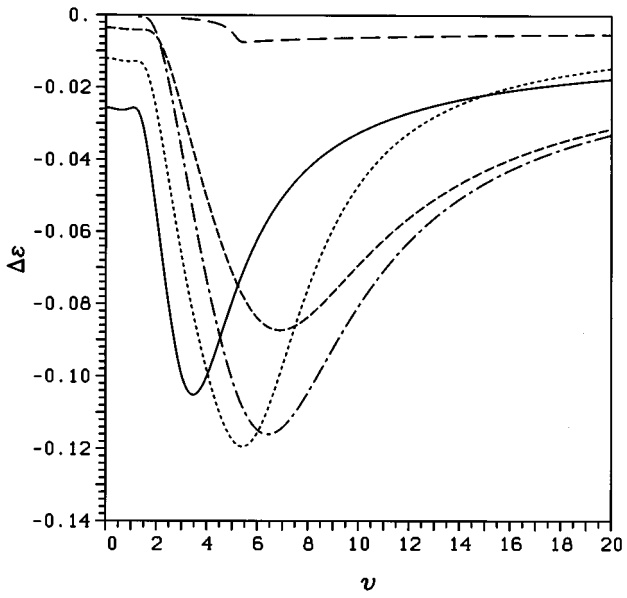

FIG. 7. Relative difference $\triangle\epsilon$ in the enhancements for a Gaussian cluster with and without internal structure as a function of the cluster velocity v in units of $\langle v_e\rangle = (v_F^2 + v_{th}^2)^{1/2}$ and for targets $T = 12$ eV, $n = 4\times10^{20}$ cm^{-3} and clusters with $N = 60$ ions and a size $\sigma = 0.2$ (long-dashed curve), 5 (solid), 10 (dashed) and $N = 200$, $\sigma = 10$ (dotted). The dashed-dotted curve belongs to $T = 0$, $n = 1.61\times10^{24}$ cm^{-3}, $N = 60$ and $\sigma = 10$. The cluster sizes σ are in units of the screening length $\lambda_0(n,T) = \langle v_e\rangle/\omega_p$, the ion charge state is $Z = 1$ in all cases.

As it becomes immediately clear by inspecting the relevant definitions, the difference in k_m^c, for the two cases, is rather small and was neglected in deriving $\triangle\epsilon$. Because $\zeta(v,\sigma,k_m^c)$ is a monotonically decreasing function of σ, the difference $\triangle\epsilon$ is always negative and the additional internal structure of the cluster reduces the enhancement. This reduction is shown not as function of σ but of the cluster velocity v in Fig. 7, where the relative changes in the enhancement $\triangle\epsilon$ are plotted for different cluster sizes and target conditions. For small clusters $\sigma \ll 1$ (long-dashed curve) the cluster behaves as pointlike, where the internal structure is of minor importance and the reduction in the enhancement takes a rather small almost constant value when the velocity is large enough, so that the electrons may resolve the structure $[\sigma/N^{1/3} \gtrsim 1/k_m^c(v)]$. For large clusters of the order of the dynamical screening length ($\sigma \sim v$, in the present scaling) pronounced reductions occur at certain velocities depending on the cluster size σ and ion number N, where the minima in $\triangle\epsilon$ are located at velocities v_m proportional to the mean interparticle spacing $\sigma/N^{1/3}$ (solid, short-dashed, and dotted curves), while in the chosen units a variation of the target conditions at given σ and N only slightly affect the v_m location (dashed-dotted curve). This reduction in the

stopping for large clusters, and medium or high velocities, is a consequence of destructive interference between the excited plasma waves, and were reported also for other types of clusters with internal structure [5,35]. A particular situation in this regard concerns very large structures, such as ion beams or bunches of ions corresponding to the limit $\sigma,N\to\infty$ for a constant ion density, that is, $\varsigma=\sigma/N^{1/3}=$const. For sufficiently large σ at a given velocity, the beam, or bunch as a whole, is larger than the dynamical screening length $\sigma\gg v$, and the long range correlation limit applies where the correlation contribution $N\zeta(v,\sigma,k_m^c)$, in the enhancement (45), vanishes like $N\zeta\sim N/\sigma^4\sim N^{-1/3}/\varsigma^4$ [cf. Eq. (40)], and the enhancement, in fact, always represents a reduction of stopping $\epsilon_\varsigma=[\zeta(v,0,k_m^c)-\zeta(v,\varsigma,k_m^c)]/\zeta(v,0,k_m)\leqslant 1$. This reduction due to destructive interference depends only on the mean ion spacing ς and increases with the density of the beam or bunch. Such behavior for beams or large clusters was already discussed in Refs. [36,37].

B. *N*-ion chains

From the rather general and statistical description of correlated stopping discussed above, we now turn to chains of ions as an example of a well defined, highly regular structure. In particular, such arrangements allow for significant interference effects of the excited wake fields and the study of N-ion chains will complete the spectrum of the basic features of correlated ion stopping.

For a chain of N (pointlike) ions with charge Ze and an equal distance L between two neighboring ions, the charge density of this configuration is

$$\rho(\mathbf{r})=Ze\,\delta(x)\,\delta(y)\sum_{n=1}^{N}\delta(nL-z), \tag{47}$$

where the extension of the chain is chosen in the z direction. The relevant product of the Fourier-transformed charge density of the chain, which enters expression (4) for the stopping power, takes the form

$$\begin{aligned}\frac{\tilde{\rho}_q(-\mathbf{k})\tilde{\rho}_q(\mathbf{k})}{Z^2e^2}&=\sum_{n=1}^{N}\sum_{m=1}^{N}\exp[ik_z(n-m)L]\\&=N+2\sum_{\nu=1}^{N-1}(N-\nu)\cos(\nu k_zL)\\&=\frac{\sin^2(Nk_zL/2)}{\sin^2(k_zL/2)}.\end{aligned} \tag{48}$$

For such highly anisotropic structures we expect, of course, a strong dependence of the stopping on the orientation of the chain with respect to its velocity. For velocities parallel to the chain, that is $\mathbf{v}=v\hat{\mathbf{e}}_z$ and $\omega=\mathbf{k}\cdot\mathbf{v}=k_zv$, the stopping per ion is given by

$$\begin{aligned}\frac{S}{N}&=Z^2S_1^c+\frac{Z^2e^2}{v^2 2\pi^2\epsilon_0}\frac{2}{N}\sum_{\nu=1}^{N-1}(N-\nu)\\&\quad\times\int_0^{k_m^c}\frac{dk}{k}\int_0^{kv}d\omega\,\omega\cos\left(\nu L\frac{\omega}{v}\right)\mathrm{Im}\left[\frac{-1}{\varepsilon(k,\omega)}\right]\\&=\frac{1}{N}\frac{Z^2e^2}{v^2 2\pi^2\epsilon_0}\int_0^{k_m^c}dk\int_0^{kv}d\omega\,\omega\frac{\sin^2\left(N\frac{\omega L}{2v}\right)}{\sin^2\left(\frac{\omega L}{2v}\right)}\\&\quad\times\mathrm{Im}\left[\frac{-1}{\varepsilon(k,\omega)}\right],\end{aligned} \tag{49}$$

with the single ion stopping S_1^c as defined in Eq. (29), while the stopping per ion for a chain extended perpendicular to its velocity ($\mathbf{v}\perp\hat{\mathbf{e}}_z$) takes the form

$$\begin{aligned}\frac{S}{N}&=Z^2S_1^c+\frac{Z^2e^2}{v^2 2\pi^2\epsilon_0}\frac{2}{N}\sum_{\nu=1}^{N-1}(N-\nu)\int_0^{k_m^c}\frac{dk}{k}\\&\quad\times\int_0^{kv}d\omega\,\omega J_0(\nu L\sqrt{k^2-(\omega/v)^2})\,\mathrm{Im}\left[\frac{-1}{\varepsilon(k,\omega)}\right],\end{aligned} \tag{50}$$

where J_0 is the Bessel function of the first kind.

To determine k_m^c for the chains according to the recipe established in Sec. II, we employ the angular average

$$\begin{aligned}\varphi_c(r)&=\frac{\langle\langle V(r)\rangle\rangle}{mv_r^2}\\&=\varphi(r)+\frac{1}{N}\sum_n\sum_{m\neq n}\frac{1}{2}\int_{-1}^{1}d\,\cos\vartheta\,\varphi(|\mathbf{r}_n-\mathbf{r}_m-\mathbf{r}|)\\&=\varphi(r)+\frac{b_0}{r}\frac{1}{N}\sum_{\nu=1}^{N-1}(N-\nu)\left[\Lambda_{\nu L}\left(r,\frac{1}{\lambda_s}\right)\right.\\&\quad\left.-\Lambda_{\nu L}\left(r,\frac{1}{\lambda_r}+\frac{1}{\lambda_s}\right)\right],\end{aligned} \tag{51}$$

with the ion spacings $\mathbf{r}_n-\mathbf{r}_m=(n-m)L\hat{\mathbf{e}}_z$, the single ion expression φ [cf. Eq. (10)], and

$$\Lambda_{\nu L}\left(r,\frac{1}{\lambda}\right)=\frac{\lambda}{\nu L}\left[\exp\left(-\frac{|r-\nu L|}{\lambda}\right)-\exp\left(-\frac{r+\nu L}{\lambda}\right)\right]. \tag{52}$$

We reconsider the enhancement $\epsilon=S/NZ^2S_1$ for the total stopping S of the parallel and transversal (perpendicular) chain Eqs. (49) and (50) with respect to the single ion stopping S_1 of isolated ions, that is, $S_1=C_2(\mathbf{r}=\mathbf{0})$, Eq. (24) with cutoff k_m Eq. (17). The resulting enhancement for a chain of $N=10$ ions with $Z=1$ is shown in Fig. 8 as function of the interion distance L for different velocities, target conditions, and orientations of the chain. In general, we recover the behavior as seen for the Gaussian cluster with a transition from vanishing enhancement $\epsilon=1$ to a constant value $\epsilon\approx N$, when L decreases from $L\gg\lambda_0$ to $L\ll\lambda_0$. This qualitative agree-

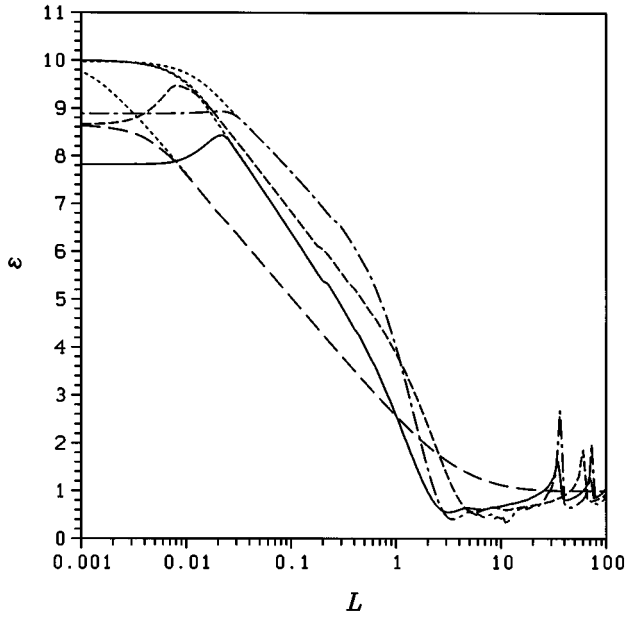

FIG. 8. Enhancement ϵ for a chain with $N=10$ ions of $Z=1$ as a function of the interion spacing L in units of $\lambda_0(n,T)=\langle v_e\rangle/\omega_p=(v_F^2+v_{th}^2)^{1/2}/\omega_p$. Transversal orientation of the chain with a velocity of $v=10$ (long-dashed curve) and parallel orientation for $v=6$ (solid) and 10 (short-dashed), all cases for a target plasmas of $T=12$ eV, $n=4\times10^{20}$ cm^{-3}, and parallel orientation with $v=6$ in a target $T=0$, $n=1.61\times10^{24}$ cm^{-3} (dashed-dotted). The velocities are scaled in units of $\langle v_e\rangle$. Again, the dotted curves display the enhancement for a pure linear behavior of the stopping when nonlinear effects are ignored.

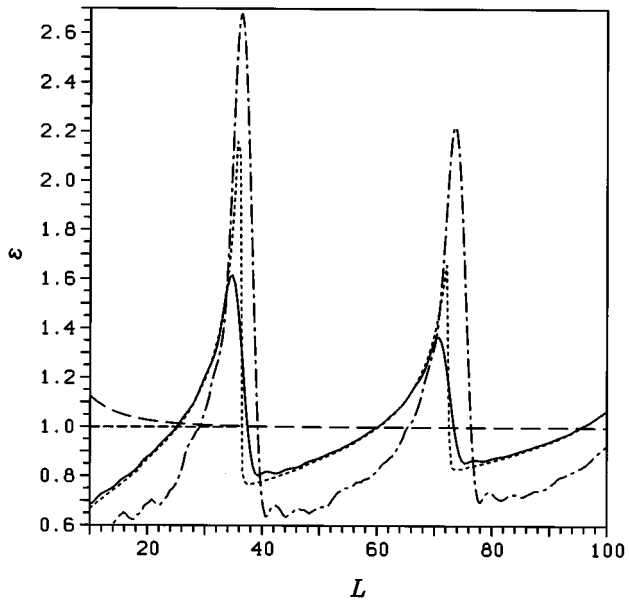

FIG. 9. Enhancement ϵ for a chain of ions with $Z=1$ and scaling as in Fig. 8 now detailed for large L. For transversal orientation, $N=10$, $v=10$ (long-dashed curve) and parallel orientation $N=10$, $v=6$ (solid), $N=100$, $v=1$ (short-dashed merging with long-dashed curve for larger L) and $N=100$, $v=6$ (dotted) for a target plasmas of $T=12$ eV, $n=4\times10^{20}$ cm^{-3}; parallel orientation, $N=10$, $v=6$ in a target with $T=0$, $n=1.61\times10^{24}$ cm^{-3} (dashed-dotted).

ment with the Gaussian cluster is almost perfect for transversal chains (long-dashed curve). The parallel chains behave quite similarly for $L<\lambda_s$, but show new additional features for large L where some resonant structures in ϵ appear. These structures are due to constructive interference of the excited plasma waves. Before we turn to further discuss these interference effects, we will remark on some additional features in Fig. 8. The onset of the increase of ϵ for decreasing L is located at the same interparticle distance [scaled in $\lambda_0(n,T)=(v_F^2+v_{th}^2)^{1/2}/\omega_p$] for the same velocity v but different target conditions (solid and dashed-dotted curves). The value for the enhancement in the limit of complete coalescence is the same for the parallel and transversal chain at the same velocity (short-dashed and long-dashed). The somehow strange behavior of the enhancement which decays again at low L for decreasing L (solid and short-dashed curves) may be an artifact of the used procedure to work out k_m^c through the spherical average (51). Such an averaging is, of course, less suitable for an anisotropic chain than for a spherical structure as the Gaussian cluster. However, this concerns only some medium range of small L, in the limit of sufficiently small L when the whole chain appears pointlike, we recover the correct enhancement of a single charge. Figure 9 shows in more detail the large L region where the resonant structures are located. No such structures are present for a transversal chain (long-dashed curve) as well as for a parallel chain at low velocities $v=1$ for which no enhancement exists in this L range. While there are (almost) no wake fields for small velocities, strong interferences of the plasma waves excited at high velocities may occur. In general these interferences are destructive and yield a reduction of stopping compared to the isolated ion value ($\epsilon<1$) such as in the region $L\approx5$–10 in Fig. 8 and between the peaks in Fig. 9. Constructive interference, which results in a significant enhancement of stopping, occurs at certain values of L, where the ions in the chain are in phase with the excited waves. Here, the wave with the strongest amplitude complies with the dispersion relation $\mathrm{Re}\omega(k)=\mathbf{k}\cdot\mathbf{v}$ and can travel in phase with the ion chain for $k=2\pi n/L$. Taking $\omega(k)$ in units of ω_p and $\mathrm{Re}\omega(k\ll1)=1$, the resonance condition $\mathrm{Re}\omega=2\pi nv/L$ for a velocity $v=6$ reads in the chosen scaling $L=12\pi n=L=37.7,75.4,\ldots$. The two first possible values agree roughly with the peak locations in Fig. 9. The discrepancy is due to the fact that we have, for nonvanishing $k\geqslant2\pi/L$, higher plasmon frequencies $\mathrm{Re}\omega(k)>1$ instead of $\mathrm{Re}\omega(k\ll1)=1$, as used for our estimate. This shifts the peaks to lower L and introduces a difference between the plasma conditions (solid and dashed-dotted curves), because the dispersion relation for $k>0$ explicitly depends on n,T in the used scaling. The plasma mode, which is selected by the dispersion relation, dominates more and more the resonance for an increasing number of ions which contribute to the wave excitations. This enforces the resonant enhancement and shifts it toward the corresponding values $L=2\pi nv/\mathrm{Re}\omega(n2\pi/L)$ (solid $N=10$ and dotted $N=100$ curves). This behavior is witnessed more distinctly in Fig. 10 as resonance with respect to the velocity for a fixed ion spacing L. The enhancement exhibits with an increasing length of the chain, a more and more pronounced

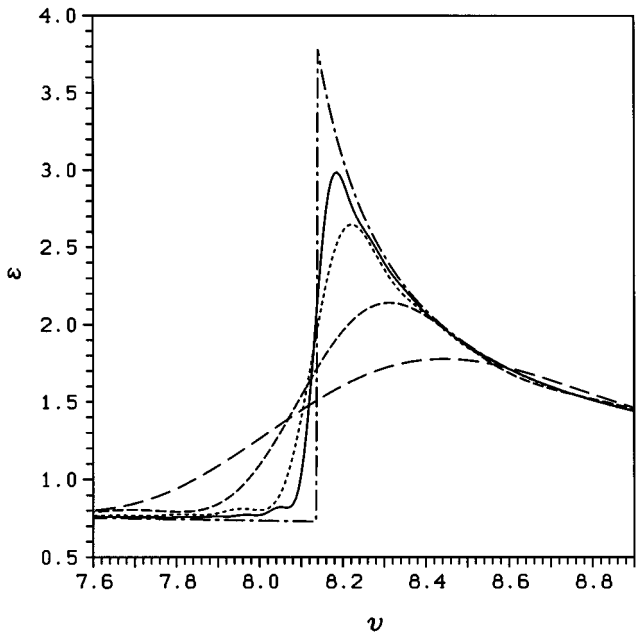

FIG. 10. Enhancement ϵ for a parallel chain of ions with $Z=1$ and interion distance $L=50$ as a function of the velocity v in a classical plasmas of $T=12$ eV, $n=4\times10^{20}$ cm^{-3} for different ion numbers $N=10$ (long-dashed curve), 20 (short-dashed), 50 (dotted), 100 (solid), and $N\to\infty$ (dashed-dotted). The spacing L is scaled in $\lambda_0(n,T)=\langle v_e\rangle/\omega_p=v_{th}/\omega_p=\lambda_D$, the velocity v in $\langle v_e\rangle=v_{th}$.

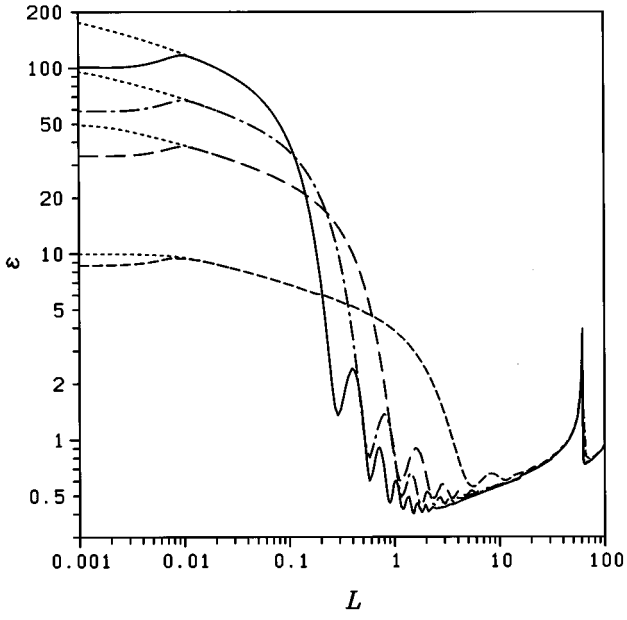

FIG. 11. Enhancement ϵ for a parallel chain of ions with $Z=1$ at a velocity $v=10$ as a function of the interion spacing L for different ion numbers $N=10$ (short-dashed curve), 50 (long-dashed), 100 (dashed-dotted), and 200 (solid). The dotted curves display again the enhancement for a pure linear behavior. Target conditions and scaling as in Fig. 10.

peak with a sharp edge for a large number of ions $N\to\infty$ towards low velocities (dashed-dotted curve). Applying the dispersion relation for this case with $L=50$ and a classical plasma $\mathrm{Re}\omega(k)\approx(1+3k^2)^{1/2}$ (with k in $1/\lambda_D$) yields $v=[(L/2\pi)^2+3]^{1/2}=8.14$ in perfect agreement with the observed edge. For lower velocities only plasma waves with shorter wave length $L/n(n>1)$ can be in phase. These waves, when exited by one ion in the chain, reach only a smaller number of further ions because they are strongly damped. For an increasing number of ions their contribution to the total stopping does not increase as well and the enhancement due to this waves is indeed reduced for growing N. For the same reason the enhancement due to the wave with length L saturates to a maximum for $N\to\infty$. Beyond the edge towards higher v, the wave with length L no longer obeys the dispersion relation but is still excited, however, with decreasing amplitude for increasing v. For velocities larger than shown in Fig. 10 the destructive interference finally results in a reduction ($\epsilon<1$) as also apparent at low velocities.

The dependence on the number of ions is addressed once more in Fig. 11 which gives an impression of the N dependence of the enhancement for parallel chains with different distances L between the ions. For large L we recover the resonant structure with its slight N dependence as discussed above, while the enhancement for small L strongly grows with increasing N (note the logarithmic scale for ϵ). Larger enhancements for larger N, however, drop down for increasing L at smaller L values than those for smaller N. This arises, because a chain no longer appears as pointlike if its total length exceeds a certain size $NL\approx1/k_m^c(v)$, which of course already happens at lower L for larger N. Together with further resonance effects this yields rather strong variations of the enhancement with respect to the ion number at ion spacings around $L\approx1$. This can be nicely demonstrated regarding the enhancement as a function of N for different fixed interion distances L as shown in Fig. 12. The enhancement grows monotonically with N at small L (long-dashed curve) but shows strong oscillations for medium L (solid and dashed). For large L outside the resonance (see Fig. 11) the enhancement rapidly decreases to values $\epsilon<1$ for small N and than remains constant for large N (not shown). This feature is opposite to the behavior within resonance (dashed-dotted curve) which saturates to $\epsilon>1$. In contrast to these features for parallel chains, the transversal chains show for all L an increase with subsequent saturation (such as the dotted curve), where the final enhancement for large N increases monotonically with shrinking distances L.

C. Embedded cubic boxes

In order to further highlight the topological dependence of correlated ion stopping, we think it instructive to add to the above highly significant examples a third one interpolating between them. This explains why we consider, in Figs. 13 and 14, three distinct target temperature stopping cases for $N=8n$ pointlike equal charges distributed on vertices on n successively embedded cubic boxes. The stopping conditions with target parameters $1\leqslant k_BT\leqslant10$ eV, $n=10^{19}$ cm^{-3}, corresponding to a classical target $\Theta\gg1$, and a projectile velocity $v=3v_{th}$, are typical of a realistic cluster ion-dense plasma interaction experiment achievable with presently existing hardware. The given arrangement of $n=1,\ldots,4$

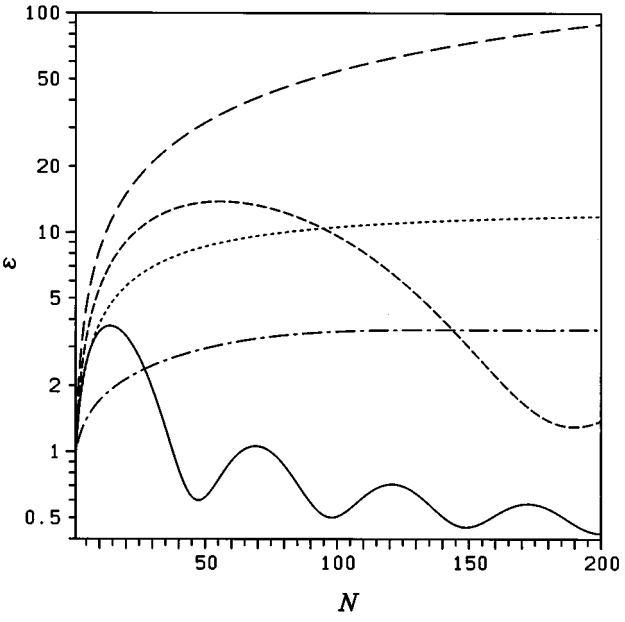

FIG. 12. Enhancement ϵ for a chain of ions with $Z=1$ and velocity $v=10$ as a function of the ion number N for different fixed interion spacings $L=0.03$ (long-dashed curve), 0.3 (short-dashed), 1.2 (solid), and 61.5 (dashed-dotted) for parallel orientation. The dotted curve exhibits transversal orientation and $L=0.3$. Target conditions and scaling as in Fig. 10.

boxes is chosen so that the largest box has an edge length equal to the target plasma screening length $\lambda_D=v_{th}/\omega_p$, the first inner box has $\lambda_D/2$, the following one $\lambda_D/4$, and the last one $\lambda_D/8$. So the presently considered enhanced stopping documents the so called intermediate range effects in the above displayed classification. The sum of binary contributions C_2, which builds up together with the single ion stopping S_1 the total stopping, can be decomposed into intrabox and interbox contributions, C^a_{ii} and C^e_{ij}, respectively,

$$S=NZ^2S_1+Z^2\sum_{\nu}\sum_{\mu\neq\nu}C_2(\mathbf{r}_{\nu\mu})$$

$$=NZ^2S_1+Z^2\sum_{i}C^a_{ii}+Z^2\sum_{i}\sum_{j\neq i}C^e_{ij}, \qquad (53)$$

where S_1, C_2, and $\mathbf{r}_{nm}$ are defined as in Eq. (23) and $\nu,\mu=1,\ldots,N$ with $N=8n$ and $i,j=1,\ldots,n$. Nonlinear effects can be assumed to be small under the present conditions and are neglected here, that is, $k^c_m=k_m$. The enhancement $\epsilon=S/NZ^2S_1$ displayed in Fig. 13 is increasing with N but at a different pace for various T. This behavior with N and T agrees qualitatively with those of the Gaussian cluster presented in Figs. 3, 5, and 6. The relative importance of the interboxes and intraboxes correlations is addressed in Fig. 14 in terms of the corresponding ratio $R=\Sigma_i\Sigma_{j\neq i}C^e_{ij}/\Sigma_i C^a_{ii}$. This ratio also increases with N but in an almost identical way for the three considered temperatures. Assuming that the binary contributions $C_2(\mathbf{r}_{\nu\mu})$ can be replaced by a mean value $\langle C_2\rangle$ we have $\Sigma_i\Sigma_{j\neq i}C^e_{ij}=8\times 8n(n-1)\langle C_2\rangle$, $\Sigma_i C^a_{ii}=8\times 7n\langle C_2\rangle$ and hence $R=8(n-1)/7$. The latter value is very close to the observed R with some deviation for $N=4\times 8=32$ due to the strong intrabox contribution C^a_{44} of the smallest box with size $\lambda_D/8$. From the found R values we may, however, conclude that the embedded cubic boxes behave in the considered regime like a compact and homogeneous arrangement despite their highly ordered and specific form. The essential message conveyed by these cubic box results is that a three dimensional arrangement of pointlike charges is likely to produce enhanced and correlated stopping. Such behavior remains obviously at variance with N-chain behavior in comparable conditions which can also produce negatively correlated stopping for some N values. The box arrangement in the above intermediate range regime behaves rather similar to the Gaussian cluster. This confirms that the Gaussian model is quite universal and useful for an averaged description of the stopping of ion debris.

IV. SUMMARY

From the examples given in the preceding section, as well as from our own studies and published investigations [5–10,18,34–36] on further cluster configurations we obtain the following general picture of correlated stopping.

A. Basic features of correlated ion stopping

1. Short range correlations

The size λ_c of the whole ion cluster is much smaller than the static screening length λ_0. More accurately, it should be smaller than the relevant spatial resolution of the electrons, that is, $\lambda_c<1/k^c_m\ll\lambda_0$, in particular, in the linear regime $\lambda_c<\lambda\!\!\!^{-}_r$ (see Sec. III A 1). This corresponds to the limit of complete coalescence where the ion clusters behave as a single pointlike ion with a charge equal to the sum of the charges of all its constituents and the stopping is characterized as follows.

The energy loss of the ion cluster grows monotonically with the number N of its constituents, that is, with increasing total charge at fixed cluster size. The corresponding increase in the enhancement is linear in N within the linear regime and less than linear $\sim N\ln(\text{const}/N)$ in the semilinear regime. The latter N dependence is deduced from the definitions (17), (22), and (38), where $k^c_m\approx k_m/N$ and reflects the kind of Bloch modification discussed in Sec. II C. It might change when, in addition, higher order response contributions are included, which could shift the N dependence again closer to a linear behavior (cf. the behavior of the charge dependence in [31]). In the essential nonlinear regime a behavior $\sim N^{0.5}$ can be proposed out of molecular dynamics simulations [38,39] for the stopping of single ions which scales approximatively $\sim Q^{1.5}$ in the total charge Q in this regime.

The correlated stopping is independent of the exact cluster structure as long as the total charge remains unchanged.

The stopping is always enhanced compared to that of uncorrelated individual ions.

The dependence of the enhancement on the ion-cluster velocity is moderate and mainly determined by the transition from the linear to the semilinear into the nonlinear regime for decreasing velocity. The related reduction of the stop-

ping, thereby, corresponds to the dependence on the total charge, i.e., on N, as outlined above.

2. Long range correlations

The size of the whole ion cluster and the typical correlation length λ_c (distances between the ions) is of same order or larger than the dynamical screening length $\lambda_s \approx \lambda_0 v$. Here every ion of the cluster acts as an individual charge with a possible correlated behavior due to the interference of the excited long ranged wake fields. This may yield enhanced or reduced stopping for constructive or destructive interference, respectively. The typical features of this type of correlated stopping are the following.

The dependence on the number N of involved ions is weak. The reduction or the enhancement of stopping due to the interferences saturates when more and more ions contribute for a fixed interionic distance λ_c. In particular, the maximal stopping per ion always remains of the order of a few times the stopping of individual ions even for a large number of ions.

In general a reduction of stopping by destructive interference occurs corresponding to a suppression of plasmon excitations with wavelengths larger than the typical distances λ_c.

Enhancements of stopping by constructive interference are possible for velocities $\mathbf{v}$ where the ion cluster is in phase with the excited plasma waves and the resonance condition $\mathrm{Re}\omega(k_c = 2\pi/\lambda_c) = \mathbf{k}_c \cdot \mathbf{v}$ is fulfilled. Because the damping of the plasma waves has to be sufficiently small these interferences can only occur for high velocities where the resonance condition yields small k_c values for which $\mathrm{Im}\omega(k_c)$ becomes negligible.

There is a strong dependence of the correlation effects on the cluster structure $\mathbf{k}_c$ and the ion-cluster velocity $\mathbf{v}$ via the resonance condition.

In addition, a strong dependence on the target conditions is witnessed as well. For nonideal plasma the interelectron correlation will reduce the plasmon mean-free path which results in a stronger damping of the plasma waves and a suppression of the interference effects [40,39].

3. Intermediate range correlations

When the cluster sizes and correlation lengths are of the order of the screening length and hence lie in between both previous regimes, the physics of correlated stopping is more complicate than in both ''pure'' cases. The intermediate regime through which transition between the above regimes takes place is mainly characterized by exhibiting simultaneous features of short range and long range correlation regimes.

The size and topology of the cluster strongly affect the dependence on the ion number N. In general, there is an increase of the enhancement with N, as for short range correlations.

Depending on the cluster structure reductions of stopping due to destructive interference may occur, but there is no enhancement by constructive interference. Therefore, the velocity dependence of correlated stopping is less pronounced than in the long range correlation regime.

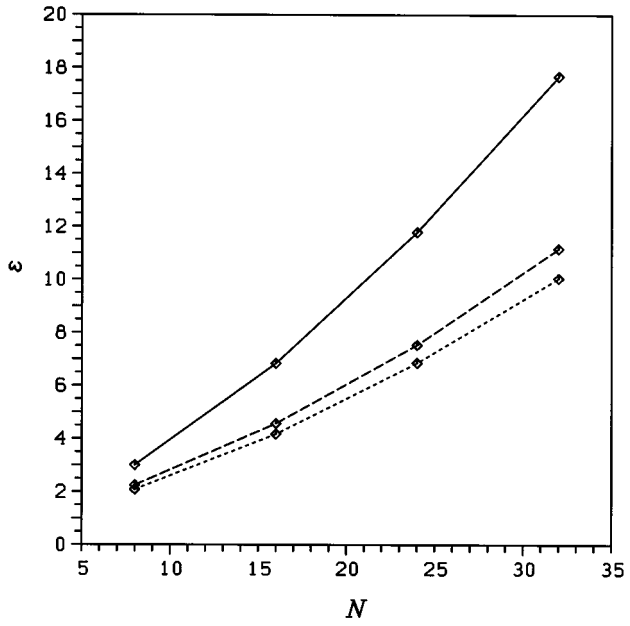

FIG. 13. Enhancement ϵ for $N = 8n$ unit charges displayed on vertices of n successively embedded cubic boxes. The cubic edges are successively λ_D, $\lambda_D/2$, $\lambda_D/4$, and $\lambda_D/8$. The overall projectile velocity is $v = 3v_{th}$, the target density is $n = 10^{19}$ cm^{-3} and the target temperatures are $T = 0.93$ eV (solid curve), 4.31 eV (dashed), and 7.37 eV (dotted).

B. Conclusions

We have critically reviewed the dielectric formulation of correlated stopping in the nonrelativistic regime. In particular, a careful distinction has been made between a Born-RPA regime with no momentum cutoff in the stopping quadrature, which advocates the standard linear regime and a quasilinear regime with short range cutoff included, corresponding to a

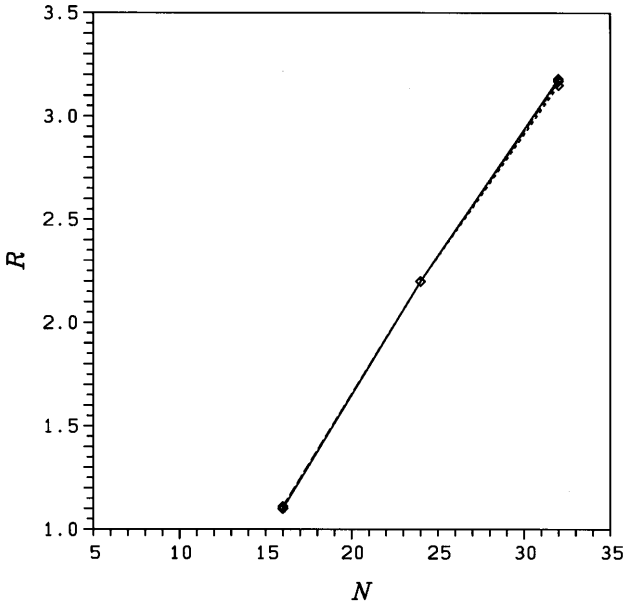

FIG. 14. Ratio R of interboxes to intraboxes correlated stopping contributions for the n successively embedded cubic boxes with $N = 8n$ unit charges and box sizes and parameters as in Fig. 13.

Bloch modification of the stopping power. We presented a scheme to derive the requested cutoffs for such a correction with arbitrary given ion arrangements. We discussed the consequences of these nonlinear effects in this quasilinear (semilinear) regime on the stopping enhancement through some selected examples. Here, the observed enhancements achievable in the semilinear regime, which are often strongly reduced compared to the linear regime, should be considered as lower bounds. They might increase again towards the linear response prediction when higher order medium polarization effects (Barkas) are included. At this point further investigations are needed to determine these contributions for the stopping of ion clusters in the semilinear coupling regime.

As demonstrated, the ratios of overall cluster size and nearest neighbor interdistance, respectively, to the plasma target screening length λ_s, allow in connection with the ratio of overall drift velocity v to the mean electron velocity $\langle v_e \rangle$ in the target to classify the expected effects connected with correlated stopping. In the case of an ion cluster with a Gaussian spherical distribution even a quantification of the stopping enhancement in terms of these ratios is provided by an approximation formula. In future work, this formula might be used to perform quantitative studies of the stopping of ion debris including the Coulomb explosion. In this context the outlined extension beyond the standard linear Born-RPA regime will become important as well. Long range effects (with respect to λ_s) as observed for an N chain parallel to v are essentially ascribed to target plasmon excitation. In this case destructive interferences may turn the correlated stopping negative and hence reduce stopping compared to the uncorrelated case. All together we showed how rich and diverse correlated stopping is and displayed the considerable qualitative and quantitative differences, as well as the common features by ion arrangements as distinct as the Gaussian spherical distribution, N chains and embedded cubic boxes.

ACKNOWLEDGMENTS

We acknowledge valuable discussions with G. Maynard and the support of this work by the Centre National de la Recherche Scientifique. G.Z. thanks the Deutsche Forschungsgemeinschaft for financial support.

[1] C. Deutsch and N. A. Tahir, Phys. Fluids B **4**, 3735 (1992).
[2] S. Eliezer, J. M. Martinez-Val, and C. Deutsch, Laser Part. Beams **13**, 43 (1995).
[3] G. Basbas and R. H. Ritchie, Phys. Rev. A **25**, 1943 (1982).
[4] N. R. Arista and A. Gras-Marti, J. Phys., Condens. Matter. **3**, 7931 (1991).
[5] M. Vicanek, I. Abril, N. R. Arista, and A. Gras-Marti, Phys. Rev. A **46**, 5745 (1992).
[6] C. Deutsch, Phys. Rev. E **51**, 619 (1995).
[7] A. Bret and C. Deutsch, Phys. Rev. E **47**, 1276 (1993).
[8] J. D'Avanzo, M. Lontano, and P. F. Bortignon, Phys. Rev. E **45**, 3574 (1993).
[9] J. D'Avanzo, E. Tome, M. Lontano, and P. F. Bortignon, Nuovo Cimento A **106**, 1803 (1993).
[10] C. Deutsch and P. Fromy, Phys. Rev. E **51**, 632 (1995).
[11] I. Nagy, A. Arnau, and P. M. Echenique, Nucl. Instrum. Methods Phys. Res. B **48**, 54 (1990).
[12] H. M. Urbassek, V. Dröge, and R. M. Nieminen, J. Phys., Condens. Matter. **5**, 3289 (1993).
[13] E. Nardi, Z. Zinamon, and D. Ben-Hamu, Nuovo Cimento **106**, 1839 (1993).
[14] E. Nardi and Z. Zinamon, Laser Part. Beams **13**, 335 (1995).
[15] D. Pines, *Elementary Excitations in Solids* (Benjamin, New York, 1973).
[16] A. L. Fetter and J. D. Walecka, *Quantum Theory of Many-Particle Systems* (McGraw-Hill, New York, 1971).
[17] C. Gouedard and C. Deutsch, J. Math. Phys. (N.Y.) **19**, 32 (1978).
[18] N. R. Arista, Phys. Rev. B **18**, 1 (1978).
[19] A. Bret and C. Deutsch, Phys. Rev. E **48**, 2989 (1993).
[20] M. Lontano and F. Raimondi, Phys. Rev. E **51**, R2755 (1995).
[21] C. Deutsch, Y. Furutani, and M. M. Gombert, Phys. Rep. **69**, 85 (1981).
[22] G. Maynard and C. Deutsch, J. Phys. (France) **46**, 1113 (1985).
[23] F. Bloch, Ann. Phys. (Leipzig) **16**, 285 (1933).
[24] N. Honda, J. Phys. Soc. Jpn. **19**, 1201 (1964).
[25] H.-S. Hahn, E. A. Mason, and F. J. Smith, Phys. Fluids **14**, 278 (1971).
[26] E. P. George and T. Hamada, Phys. Lett. **67A**, 369 (1978).
[27] L. de Ferrariis and N. R. Arista, Phys. Rev. A **29**, 2145 (1984).
[28] L. Bönig and K. Schönhammer, Phys. Rev. B **39**, 7413 (1989).
[29] I. Nagy and A. Bergara, Nucl. Instrum. Methods Phys. Res. B **115**, 58 (1996).
[30] T. Peter and J. Meyer-ter-Vehn, Phys. Rev. A **43**, 1998 (1991).
[31] J. A. Golovchenko, D. E. Cox, and A. N. Goland, Phys. Rev. B **26**, 2335 (1982).
[32] H. Esbensen and P. Sigmund, Ann. Phys. (N.Y.) **201**, 152 (1990).
[33] J. M. Pitarke, R. H. Ritchie, and P. M. Echenique, Phys. Rev. B **52**, 13 883 (1995).
[34] J. D'Avanzo, M. Lontano, and P. F. Bortignon, Phys. Rev. A **45**, 6126 (1992).
[35] F. J. Perez-Perez, I. Abril, R. Garcia-Molina, and N. R. Arista, Phys. Rev. A **54**, 4145 (1996).
[36] E. M. Bringa and N. R. Arista, Phys. Rev. E **52**, 3010 (1995).
[37] G. Zwicknagel and C. Deutsch, Laser Part. Beams **14**, 749 (1996).
[38] G. Zwicknagel, Ph.D. thesis, Universität Erlangen, 1994 (unpublished).
[39] G. Zwicknagel, C. Toepffer, and P.-G. Reinhard, Laser Part. Beams **13**, 311 (1995).
[40] J. C. Ashley and P. M. Echenique, Phys. Rev. B **35**, 8701 (1987).